Deoxygenation of wheat straw fast pyrolysis vapors using HZSM-5, Al2O3, HZSM-5/Al2O3 extrudates, and desilicated HZSM-5/Al2O3 extrudates

Eschenbacher, Andreas; Jensen, Peter Arendt; Henriksen, Ulrik Birk; Ahrenfeldt, Jesper; Li, Chengxin; Duus, Jens Øllgaard; Mentzel, Uffe Vie; Jensen, Anker Degn

Published in:
Energy & Fuels

Link to article, DOI:
10.1021/acs.energyfuels.9b00906

Publication date:
2019

Document Version
Peer reviewed version

Biofuels and Biomass

Deoxygenation of wheat straw fast pyrolysis vapors using HZSM-5, AlO, HZSM-5/AlO extrudates, and desilicated HZSM-5/AlO extrudates

Andreas Eschenbacher, Peter Arendt Jensen, Ulrik Birk Henriksen, Jesper Ahrenfeldt, Chengxin Li, Jens Ø. Duus, Uffe Vie Mentzel, and Anker Degn Jensen

Energy Fuels, **Just Accepted Manuscript** • DOI: 10.1021/acs.energyfuels.9b00906 • Publication Date (Web): 24 May 2019

Deoxygenation of wheat straw fast pyrolysis vapors using HZSM-5, Al_2O_3, HZSM-5/Al_2O_3 extrudates, and desilicated HZSM-5/Al_2O_3 extrudates

Andreas Eschenbacher[a], Peter Arendt Jensen[a], Ulrik Birk Henriksen[b], Jesper Ahrenfeldt[b], Chengxin Li[c], Jens Øllgaard Duus[c], Uffe Vie Mentzel[d], and Anker Degn Jensen[a]

[a]DTU Chemical Engineering, Technical University of Denmark, Søltofts Plads 229, 2800 Kgs. Lyngby, Denmark

[b]DTU Chemical Engineering, Technical University of Denmark, Frederiksborgvej 399, 4000 Risø, Denmark

[c]DTU, Chemistry, Technical University of Denmark, Kemitorvet Building 207, 2800 Kgs. Lyngby, Denmark

[d]Haldor Topsøe A/S, Haldor Topsøes Allé 1, 2800 Kgs. Lyngby, Denmark

KEYWORDS Wheat Straw; Fast Pyrolysis; Bio-oil; Deoxygenation; NMR; HZSM-5, Al_2O_3; Desilication; Zeolite;

ABSTRACT

HZSM-5 extrudates, its two constituents (HZSM-5 zeolite and alumina binder), and SiC for reference were tested after steam treatment for the upgrading of wheat straw fast pyrolysis (FP) vapors from an ablative bench scale system. In addition, mesoporosity was added to the HZSM-5 crystals of the zeolite/Al_2O_3 extrudates by desilication, which decreased the microporous volume and led to enhanced weak acidity and less strong acidity compared to the parent extrudates. For increasing biomass-to-catalyst ratios (w/w, B:C), oils were collected and analyzed for elemental composition, total acid number (TAN), moisture, molecular weight, evaporation characteristics, and chemical composition by gas chromatography mass spectrometry with flame ionization detection (GC-MS/FID), ^{1}H nuclear magnetic resonance (NMR), ^{13}C NMR, and two-dimensional heteronuclear single-quantum correlation (2D HSQC) NMR. Compared to Al_2O_3, catalysts containing HZSM-5 promoted aromatization and limited the coke formation due to its shape selective micropores. Nevertheless, Al_2O_3 was effective in deoxygenation. At B:C ~7, 23 wt-% carbon/25 % energy recovery in the oil fraction was obtained while reducing the oxygen content by 45 % relative to a thermal reference oil fraction obtained over a SiC bed. As such, Al_2O_3 offers certain benefits compared to HZSM-5 based catalysts due to its lower cost and better hydrothermal stability with respect to acidity. At a catalyst temperature of 500 °C, the introduction of mesopores to HZSM-5 extrudates led to higher energy recovery as oil compared to the parent HZSM-5 extrudates. At B:C = 6.3, 23 wt-% carbon/26% energy recovery in the oil phase was achieved while removing 45% of the oxygen functionalities relative to the thermal reference bio-oil. Compared to deep deoxygenation for direct hydrocarbon production, mild deoxygenation improved the energy recoveries of the oil fractions and appears viable for pretreating pyrolysis vapors before co-processing bio-oils with fossil oil in refineries.

Introduction

Co-feeding biomass-derived fast pyrolysis oils with fossil oil in oil refineries can decrease our dependence on crude oil and increase the share of renewables in the transport sector. Fast pyrolysis requires short gas residence times (less than 2 s), high heating rates (>500 °C/s), moderate temperatures (400–700 °C), and low pressures (1–5 atm) in order to obtain a high oil yield[1]. Advantageously, fast pyrolysis processes are generally flexible with respect to biomass feedstocks[1–3]. The pyrolysis oil is comprised of hundreds of different oxygenated species which, unfortunately, render the oil acidic and unstable[4]. In order to process biomass derived pyrolysis-oils at oil refineries, a reduction of the oil's oxygen content and acidity is required[5]. Deoxygenation can be obtained by direct upgrading of the pyrolysis vapors under atmospheric conditions over solid acid catalysts. HZSM-5 with a molar Si/Al range of 11–40 is considered among the most suitable for production of aromatics and gasoline range products when upgrading biomass derived pyrolysis vapors since the shape selective micropores improve the selectivity to aromatics and limit coke formation[6,7]. Nevertheless, rapid deactivation by coking occurs requiring frequent regeneration which in turn may promote catalyst deactivation by irreversible dealumination.

Due to the small size of HZSM-5 crystals (<1 μm), binders are required to shape the catalyst and ensure sufficient physical strength to reduce attrition for both fixed bed and particularly fluid bed operation as well as catalyst transport and reactor filling. Typical binders include clays, silica (SiO_2), and alumina (Al_2O_3). Besides the benefit of the binder on the catalyst's mechanical strength, it changes the catalyst´s physical and chemical characteristics such as porosity and acidity, thereby influencing coke formation[8]. Acidic alumina or silica-alumina are used as catalysts to pre-crack bulky hydrocarbon species in fluid catalytic cracking (FCC). While the influence of binder on catalyst activity and coking has been thoroughly studied for FCC and the methanol-to-gasoline ((MTG) and methanol-to-olefins (MTO) processes, only few studies investigated the

deoxygenation of biomass pyrolysis vapors and its model compounds with HZSM-5/Al_2O_3 extrudates. When using HZSM-5/γ-Al_2O_3 as MTO catalyst, it has been shown that the binder is not as active as the zeolite but it provides additional porosity and acidity, and enhances the hydrothermal stability of the catalyst[9–11].

Iisa et al.[12] tested Al-rich HZSM-5 (Si/Al = 15) with 10 wt-% alumina for upgrading of pine pyrolysis vapors in a Py-GCMS/FID system, both in in-situ mode (B:C = 0.2) and in an ex-situ bed configuration at B:C = 0.5 and 2. In comparison to catalysts with clay and silica binders, the catalyst with alumina gave higher coke yields and deactivated faster.

Increased coking with HZSM-5/Al_2O_3 is consistent with higher coking and deactivation rates in propane aromatization reported for gallosilicates (MFI structure) with alumina binder compared to kaolin or silica binder[8], which was attributed to the increased acidity on the zeolite crystal surface due to the creation of new zeolite acidic sites.

Du et al.[13] pyrolyzed miscanthus in an *in-situ* PyGC mixed with pure HZSM-5 (Si/Al = 40), HZSM-5/Al_2O_3 and a commercial Al_2O_3 binder. Due to the dilution of zeolite by the Al_2O_3 binder, relatively less mono-aromatic hydrocarbons were formed. In the same work, toluene was pyrolyzed as model compound and coke yields increased with increased binder content. Upon co-feeding of propylene with toluene, it was found that the Lewis acidity of the Al_2O_3 binder promotes alkylation and cyclization of propylene, leading to enhanced benzene production. While the Lewis acidity of the binder enhanced the coke production, the coke was less condensed and combusted at lower temperature.

Very recently, Pala et al.[14] reported on the ex-situ upgrading of pine FP vapors (feeding rate 220 g/h) over a fixed bed of HZSM-5/Al_2O_3 extrudates (50 wt-% each) up to B:C = 17. With increased B:C ratio, the organic yields increased and a clear breakthrough of oxygenates and decrease of

aromatics resulted. While porosity was restored upon regeneration, a 55% loss in Lewis acidity and a 67% loss in Brønsted acidity was observed compared to the fresh extrudate.

While catalytic fast pyrolysis (CFP) benefits from the zeolite's shape selective pore structure and Brønsted acidity it also comes at a higher cost compared to the binder material and the zeolite is known to suffer from dealumination under hydrothermal conditions. If sufficient deoxygenation and stabilization of the bio-oil could be achieved over the alumina binder itself, which has higher stability towards steaming, its use may offer economic advantages over HZSM-5 based catalysts and allow faster regeneration (coke-combustion) at harsher conditions. Alumina has been tested by others for deoxygenation of biomass derived fast pyrolysis vapors[15–19]. Samolada and coworkers[19] reported that using γ-Al_2O_3 gave about 2-3 times higher coke yields compared to HZSM-5 when converting synthetic bio-oil over a catalyst fixed bed at 500 °C. For upgrading of beech pyrolysis vapors at a bench-scale fixed bed reactor with several alumina and ZSM-5 catalysts, Stephanidis et al.[15] reported increasing coke yields on alumina with increasing surface area and overall higher coke yields compared to ZSM-5 containing catalysts, in agreement with Samolada et al.[19]. The alumina catalysts with high surface area showed high selectivity towards hydrocarbons, but at low organic liquid yield (5.5 wt-% of biomass). Zhang et al.[20] tested physical mixtures of a HZSM-5 based FCC additive (Si/Al = 40) and alumina for catalytic pyrolysis of rice stalks in a fluidized bed reactor. Increased aromatic and olefin yields and reduced coke were obtained, when 10% alumina was mixed with HZSM-5. The benefit was explained by cracking of the large-molecule oxygenates into small-molecule oxygenates, which could then be converted by the HZSM-5 based catalyst into olefins and aromatics (40% increase compared to HZSM-5 only). Higher alumina additions (50%) decreased the mono-aromatics yields to values below those obtained by HZSM-5.

Wang et al.[21] reported the use of a spray-dried alumina-based catalyst in a fluidized-bed system at B:C ratios of 0.25–0.6 to study seven types of woody and herbaceous feedstocks (including wheat straw). The oxygen contents of the phase separated oil fraction from all feedstocks were below 20 wt-% at yields between 14–20.8 wt-% of biomass, indicating a good deoxygenation performance. In a later study, Mante et al.[22] reported the CFP of loblolly pine with γ-Al_2O_3, both in lab and pilot plant scale where oils with 16 and 23 wt-% oxygen (d.b.) were obtained at yields of 8.9 and 10.9 wt-% of biomass respectively.

The benefit of mesoporous HZSM-5 for CFP of biomass was demonstrated by several groups[23–26], but has not yet been demonstrated for hierarchically structured zeolite extrudates. Extrudates of hierarchical HZSM-5 and different binders (silica, acid-dispersed boehmite, kaolin, and attapulgite) were tested by Michels et al.[9] for the conversion of methanol to hydrocarbons. The hierarchical HZSM-5 powder exhibited a lifetime double that of the conventional zeolite. Shaping the hierarchical HZSM-5 powder with silica or boehmite reduced the catalyst lifetime, while catalyst lifetime was extended upon shaping with kaolin and attapulgite binder.

Michels[27] reported that leaching of HZSM-5 granules (Si/Al = 39, attapulgite clay binder) for 30 min with 0.2M NaOH at 65 °C led to the disintegration of the bodies, which was associated with the weakening of interparticle interactions due to hydrolysis caused by the alkaline solution. Michels therefore chose to desilicate the HZSM-5 crystals prior to mixing with the binder. In contrast, Groen et al.[28] had earlier reported the successful desilication of HZSM-5/Al_2O_3 extrudates for 30 min with 0.8M NaOH at 65 °C, employing a mass ratio of leaching solution to zeolite (L/S) of 10. The binder consisted of mostly alumina, but the blending ratio used in the manufacturing of the extrudates was not disclosed. The desilication did not lead to disintegration of the extrudates and Groen et al.[28] even reported an enhanced hardness of the alkaline-treated

extrudates, which was tentatively attributed to the partial dissolution of the zeolite crystals and alumina, leading to a more integrated binder/crystal composite.

The purpose of this investigation is to compare the performance of HZSM-5 (Si/Al = 40), with the alumina binder itself and extrudates comprised of 65 wt-% HZSM-5 and 35 wt-% γ-Al_2O_3 binder. The effect of catalyst amount and conversion capacity in terms of increasing B:C ratio on the product distribution and oil properties was studied in detail. To the best of our knowledge, the performance of extrudates comprised of hierarchical HZSM-5 and alumina binder has not been reported for in-situ or ex-situ CFP. We therefore investigated if auxiliary mesoporosity can be added to the HZSM-5 crystals of the shaped HZSM-5/Al_2O_3 extrudates by alkaline leaching without disintegration of the technical shaped bodies, and how the desilication affects the extrudates' deoxygenation performance.

Experimental

Pyrolysis. The experimental set-up and the characteristics of the straw feedstock were described previously[29]. Straw was fed at ~200 g/h to an ablative fast pyrolysis unit, operated at 530 °C. Char separation was achieved by cyclones (450 °C) and hot gas filtration using a ceramic filter candle (350 °C) upstream of the ex-situ located catalytic fixed bed, which contained 24–260 g catalyst. Five different liquid product fractions were obtained from each experiment. At the first condensation stage operated at 4 °C using a series of metal impingers, the liquid product phase separated into an oil fraction (4 °C OF) and a water-rich fraction (4 °C WF). The 4 °C condensation stage was followed by an electrostatic precipitator (ESP) operated at room temperature, which collected a single oil phase (ESP OF). The final condensation stage consisted of a series of dry glass impingers cooled to −60 °C by an external dry ice/ethanol bath. The liquid collected at −60 °C separated in an organic rich (−60 °C OF) and an aqueous fraction (−60 °C WF). The total liquid

product (excluding the moisture introduced from biomass) is defined as the sum of reaction water, the organics contained in the three OF, and the organics contained in the two WF. The sum of organic content obtained in the OF and WF will be referred to as organic liquid (OL). The noncondensable gases (NCG) were analyzed using continuous NDIR gas analyzers and GC-TCD/FID. The gas products were grouped into C_{2-3} olefins, C_{1-3} alkanes, CO, CO_2, and hydrogen.

Previous experience with fast pyrolysis of wheat straw using the centrifugal reactor[30] resulted in uncertainties (±2 standard deviations) of 0.7, 0.7, 3.8, and 1.5 wt % for the product yields (daf basis) of organic liquid, reaction water, char, and gas, respectively.

Catalyst Preparation. Conventional HZSM-5 with Si/Al ~40, was purchased from Zeolyst Int. (CBV 8014) and is abbreviated CBV80. The SiC, the extrudates of the γ-Al_2O_3 binder (same as used for preparation of the shaped HZSM-5/Al_2O_3), and the HZSM-5 extrudates (Extr) consisting of 65% HZSM-5 (same Si/Al ratio as CBV80) and 35% Al_2O_3 binder were provided by Haldor Topsøe A/S. A particle size of 250–850 μm was chosen for SiC and all catalysts, i.e. the CBV80 powder was pelletized, crushed and sieved while the shaped HZSM-5/Al_2O_3 and Al_2O_3 extrudates were only crushed and sieved. All catalysts were steamed prior to their use by injecting water (2 ml/min) into a preheated nitrogen stream (4 Nl/min) and passing the steam (~30 vol.-%) for 5 h through the fixed bed of catalyst kept at 500 °C under atmospheric pressure conditions.

The preparation of mesoporous HZSM-5 extrudates was performed akin to the procedure reported for desilication of HZSM-5 (Ref Fuel Proc. Tech. manuscript). Prior to preparation of a larger batch, the desilication of extrudates was tested with 0.3M and 0.5M NaOH solutions, respectively. Leaching was conducted under stirring for 30 min at 65 °C. After washing and drying overnight at 105 °C, the mesoporous HZSM-5 extrudates (abbr. mesoExtr) were subjected to an acid wash for 6 h at 65 °C with 0.02M HCl in order to remove Al debris potentially blocking pore

mouth entries[31,32]. After washing and drying overnight, the mesoExtr were ion-exchanged with 1M NH_4NO_3 at 80 °C for 24 h. After washing and drying, the protonated form was obtained by calcination under dry air for 5 h at 550 °C. For the catalytic tests, a larger amount of mesoExtr was prepared by leaching 100 g of extrudates in 10 L of 0.3M NaOH at 65 °C for 30 min. The solid yield after leaching was 90%. Acid wash, ion exchange and calcination were performed as described above. The procedure was repeated to obtain sufficient amount of mesoExtr for the catalytic test (140 g).

Vapor Upgrading. The experiments were stopped once a certain amount of wheat straw was fed corresponding to the desired mass ratio of dry and ash-free (daf) biomass to catalyst (B:C). About 24-36 g of catalyst was used to cover B:C ratios above ~6 and packed into an externally heated reactor tube (ID = 20 mm, length = 190 mm), resulting in a bed height of ~19 cm for most catalysts (17.5 cm for the HZSM-5/Al_2O_3). A 5–10 times higher mass of catalyst was used to investigate B:C ratios <10 using a larger externally heated reactor (ID = 67 mm, length = 250 mm), resulting in a bed height of 8-10 cm with the exception of HZSM-5/Al_2O_3 (15 cm). The smaller reactor scale allowed to investigate higher B:C ratios within a reasonable timeframe while the larger reactor scale ensured that sufficient oil product was collected at all condensation stages at low B:C ratios. Due to the differences in vapor residence time (see **Table 1**), the performance of the catalysts should be compared for each reactor size, and not across the two reactor scales.

The operation for extended run-times improved the mass balance; in particular, the yield of non-condensable gases (NCG) may be under-represented for short run-times due to a gas-sampling interval of >10 min. For oxidative regeneration of the catalysts, nitrogen was mixed with air to obtain ~2 vol-% O_2 (total flowrate 2 Nl/min) and the temperature was ramped from 250 °C to ~550

°C at 1 °C/min. The final temperature was held for several hours and the nitrogen was stepwise replaced by air until no more CO and CO_2 was measured in the effluent gas stream.

Table 1 numbers the experimental runs and summarizes the main operating conditions and obtained mass balances of the reported results. The pyrolysis was conducted at 530 °C with 8 Nl/min nitrogen as carrier gas, which gave <1.1 s gas residence time within the pyrolysis zone. The cyclones and hot gas filtration upstream of the catalytic bed were operated at 450 °C and 350 °C, respectively. The catalytic reactor was operated at 500 °C, unless noted otherwise. Two non-catalytic tests were performed with i) an empty catalytic reactor at 500 °C (not shown in **Table 1**) and ii) 95 g of SiC (500 °C) as a highly inert solid. The mass balances were in the range 92–98%. The history of the catalyst in terms vapor upgrading and regeneration by coke combustion is indicated by the suffixes "u" and "r" respectively, with the superscript numbers indicating the number of each. As an example, Al_2O_3-st-u^2-r^2 indicates that the alumina catalyst was steamed and underwent two upgrading and regeneration cycles.

Table 1. Process conditions and mass balances for runs employing steamed HZSM-5 (CBV80-st), steamed alumina-binder (Al_2O_3-st), steamed HZSM-5 extrudates (Extr-st), and steamed mesoporous HZSM-5 extrudates (mesoExtr-st) as catalyst. The suffixes 'st', 'u', and 'r' to the catalyst designation indicate steaming, upgrading, and regeneration procedures, with the superscript number indicating the number of each treatment.

Experiment number	Catalyst	Mass of catalyst [g]	Catalyst bed volume [cm^3]	Residence time [s] (STP)	T [°C]	Biomass feeding rate [g/min]	B:C range	Mass balance (%)
S0	SiC	95	60	0.4	500	2.7	0–11	95
Z801	CBV80-st-u-r	140	300	2.1	500	3.2	0–2.8	97
Z802	CBV80-st	140	300	2.1	500	2.4	0–4.5	94
Z803	CBV80-st-u-r	24	60	0.4	500	2.8	0–9.9	93
Z804	CBV80-st	24	60	0.4	500	2.1	0–17	97
A001	Al_2O_3-st	178	300	2.1	500	3.2	0–2.2	95
A002	Al_2O_3-st-u-r	178	300	2.1	500	3.2	0–7.3	95
A003	Al_2O_3-st-u^2-r^2	178	300	2.1	450	3.4	0– 6.2	98
A004	Al_2O_3-st	36	60	0.4	500	3.2	0–6.0	95
AZ801	Extr-st	260	550	3.8	500	0.8	0–1.9	n.d.
AZ802	Extr-st-u	260	550	3.8	500	2.5	1.9 -5.6	94
AZ803	Extr-st	26	55	0.4	500	2.8	0–6.4	98
AZ804	Extr-st-u-r	26	55	0.4	500	2.7	0–13	94
mAZ801	mesoExtr-st-u-r	140	300	2.1	500	3.6	0–2.1	92
mAZ802	mesoExtr-st-u^2-r^2	140	300	2.1	450	3.4	0–6.1	96
mAZ803	mesoExtr-st	140	300	2.1	500	3.5	0–6.3	96
mAZ804	mesoExtr-st-u^3-r^3	140	300	2.1	550	3.5	0–6.4	98
mAZ805	mesoExtr-st	28	60	0.4	500	3.7	0–10.6	94

Catalyst Characterization. The methodology for catalyst characterization has been outlined recently[29]. Besides the samples exposed to hydrothermal conditions, also the freshly calcined samples were characterized by Ar and N_2 physisorption for analysis

of micro and mesopores, respectively. TEM images were acquired using a Tecnai T20 G2 (200 kV acceleration voltage). Samples were prepared by dispersion of the sample in methanol in an ultrasonic bath, after which drops of the suspension were placed on a copper grid containing a lacey carbon film and dried over-night.

TPD of NH_3 was performed in order to quantify the total acidity of the catalysts. The two characteristic peaks desorbing at ~209 °C and ~407 °C of the acid strength distribution obtained by NH_3-TPD were fitted (Gaussian) in order to obtain the distribution between weak (W) and strong (S) acidity. Others have ascribed the desorption peak of strong acid sites at around 400 °C to strong Brønsted acid sites associated to framework Al atoms[33]. TPD of Ethylamine was employed in this study for direct quantification of the Brønsted acidity[34,35].

In order to investigate if the hot gas filtration upstream of the zeolite bed prevented the transfer of biomass indigenous alkalines that would poison the acid sites, some catalysts were analyzed for their elemental composition (Si, Al, K, Ca, Mg, and Na) by XRF before and after their repeated use and regeneration.

Oil Characterization. The methodology for oil characterization has been reported previously[29]. Karl Fischer titration, elemental analysis and GC-MS/FID was conducted for the mixture of water fractions obtained at the 4 °C and −60 °C stage (sum WF), and the mixture of oil fractions (sum OF) obtained at the 4 °C, ESP, and −60 °C condensation stage. The mixtures were prepared gravimetrically according to the yield of each fraction at each condensation stage. Please note that due to the high water content of the aqueous fractions only their carbon content could be accurately determined by elemental analysis. Since the sulfur concentration was below the detection limit of the elemental analyzer, some oils were subjected to total sulfur analysis according to ASTM method D5453. TAN and evaporation behavior was determined for the mixed OF. A heating ramp

of 10 °C/min was used for the investigation of the oils' evaporation behavior in a thermogravimetric analyzer (TGA, Netzsch Jupiter449F1). The temperature was ramped to 500 °C under N_2 atmosphere and held for 30 min. The solid remains from the TGA simulated distillation curves combusted uniformly for all oils investigated within a temperature range of 520–710 °C after switching to oxidative atmosphere (10 Vol-% O_2) and ramping from 300 to 1000 °C at 10 °C/min (not shown).

Results

Physicochemical catalyst characterization. Isotherms from high-resolution low temperature Argon pore characterization (87 K) for the fresh (unsteamed) HZSM-5, the alumina binder, the extrudates with HZSM-5, and the desilicated extrudates are shown in **Figure 1**a. Acidity characterization by NH_3-TPD was performed for the calcined and steam treated catalysts, and after several reaction/regeneration cycles. The NH_3 desorption profiles are provided as ESI, Figure S1–S4. **Table 2** provides an overview of the catalysts' textural properties, their acidity characterization (both total and Brønsted acidity), and their molar Si/Al ratio and Na content (determined by XRF). As the differences in textural properties between the freshly calcined catalysts and the recovered catalysts after both steaming and reaction/regeneration appear small, the textural properties of the steamed-only samples were not investigated in detail.

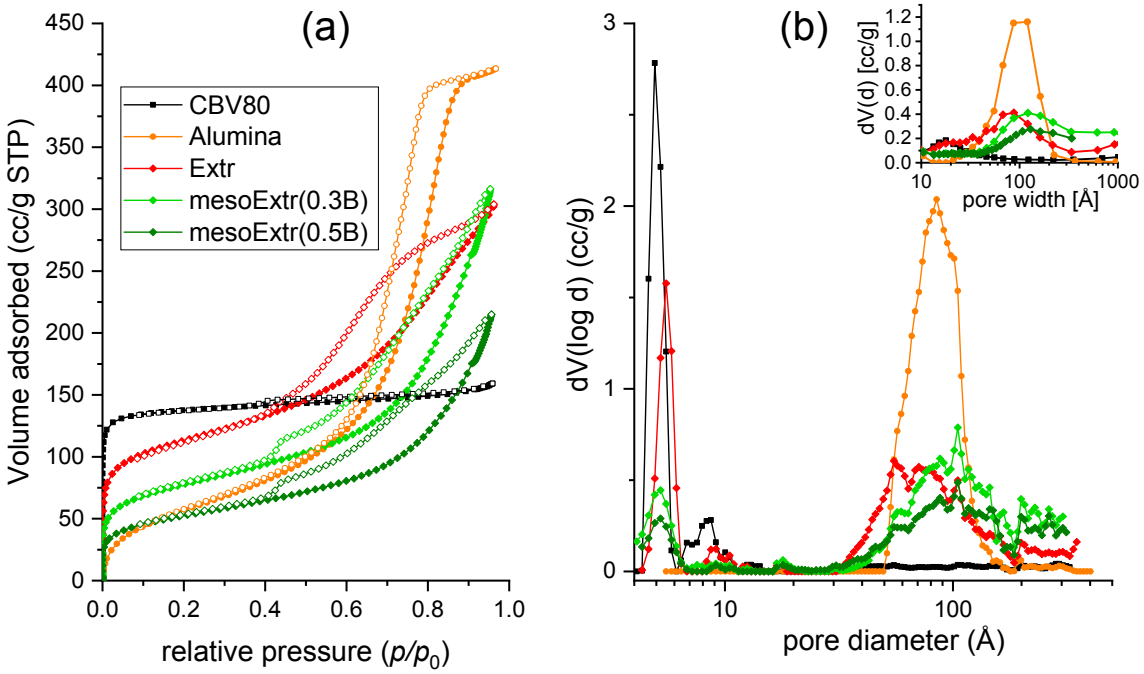

Figure 1. High-resolution low temperature Argon pore characterization (87 K) for HZSM-5, alumina binder, extrudates thereof, and desilicated extrudates. Characterization shown for calcined catalysts (unsteamed). Legend in (a) applies for both figures. Filled symbols in (a) refer to adsorption branch while open symbols refer to desorption branch of isotherms. (b) Shows the pore size distribution (PSD) obtained from applying the NL-DFT model to the adsorption branch of the Argon isotherm. Insert in (b) shows PSD obtained from applying the BJH model to adsorption branch of isotherms from N_2 physisorption.

Table 2. Physicochemical characterization of the parent HZSM-5 (CBV80-st), the alumina-binder, the HZSM-5 extrudates, and the desilicated HZSM-5 extrudates. V_{micro} and S_{micro} were determined by high-resolution low temperature Argon physisorption (87 K), while all other textural parameters were derived from nitrogen adsorption data. Total acidity was determined by NH_3-TPD. The Brønsted acidity was quantified by Ethylamine-TPD. The suffixes 'st', 'u', and 'r' to the catalyst designation indicate steaming, upgrading, and regeneration procedures, with the superscript number indicating the number of each treatment. CBV80-st-u^2-r^2, Al_2O_3-st-u^3-r^3, Extr-st-u-r, and mesoExtr-st-u^4-r^4 refer to the catalyst obtained after experiment Z801, A003, AZ802, and mAZ804 (see **Table 1**).

Sample	V_{micro} [cc/g]	S_{micro} [m^2/g]	V_{meso} [cc/g]	S_{meso} [m^2/g]	V_{total} at p/p_0 =0.99	BET (N_2) m^2/g	Total Acidity [mmol NH_3/g]	Brønsted Acidity [mmol NH_3/g]
CBV80	0.20	1585	0.06	51	0.24	431	0.520	n.d.
CBV80-st	n.d.	n.d.	n.d.	n.d.	n.d.	n.d.	0.335	0.150
CBV80-st-u^2-r^2	0.19	1427	0.08	70	0.30	419	0.387	0.135
Al_2O_3	0	0	0.56	268	0.55	228	0.301	0.061
Al_2O_3-st	0	0	0.53	235	0.52	201	0.313	n.d.
Al_2O_3-st-u^3-r^3	0	0	0.49	212	0.48	181	0.308	n.d.
Extr	0.12	865	0.31	178	0.46	395	0.486	n.d.
Extr-st	n.d.	n.d.	0.32	171	0.45	376	0.385	0.154
Extr-st-u-r	0.11	859	0.33	177	0.44	353	0.338	n.d.
mesoExtr	0.07	502	0.37	134	0.50	248	0.561	n.d.
mesoExtr-st	n.d.	n.d.	0.38	153	0.49	251	0.330	0.163
mesoExtr-st-u^4-r^4	n.d.	n.d.	0.39	153	0.50	243	0.325	0.101

Pore characterization. As expected, the fresh HZSM-5 component of the extrudate mainly contains micropores (0.2 cc/g), while the fresh Al_2O_3 binder is purely mesoporous. It is noted that the application of the BJH method from N_2 adsorption data calculates ~0.01 cc/g higher mesopore volume (V_{meso}) compared to the total volume (V_{total}). This may be attributed to the lower resolution

of the N_2 adsorption points, which leads to uncertainties in the linear interpolation between data points. Application of the NL-DFT model to the argon adsorption isotherms obtained for the fresh Al_2O_3 binder indicates V_{total} = 0.53 cc/g and V_{meso} = 0.52 cc/g.

The small amount of mesoporosity in the HZSM-5 (0.06 cc/g) is expected to result from narrow voids between agglomerated crystals (inter-crystallite porosity). Note the different shapes of adsorption isotherms (**Figure 1**), which shows the high uptake of HZSM-5 at low relative pressure, whereas alumina shows a major uptake at p/p_0 ~0.7. The HZSM-5 exhibited a Type I(a) isotherm, while Al_2O_3 showed a Type IV(a) isotherm according to IUPAC classifications[36]. The hysteresis loop of Al_2O_3 may be characterized as Type H1, in agreement with its narrow range of uniform mesopores, while the isotherm of HZSM-5/Al_2O_3 shows characteristics of both constituents and a H4 hysteresis loop. The low slope region in the middle observed for parent and desilicated HZSM-5/Al_2O_3 indicates the presence of multilayer adsorption[36], as others have observed for desilicated HZSM-5[37].

The fresh HZSM-5 extrudate contains a micropore volume (V_{micro}) of 0.12 cc/g and a mesopore volume (V_{meso}) of 0.31 cc/g. The steaming and two reaction-regeneration cycles lead to a slight decrease in V_{micro} and an increase in mesoporosity for CBV80. For the Al_2O_3, a decrease in pore volume from 0.55 to 0.48 cc/g was observed accompanied by a pronounced decrease in BET surface area by 21%. In contrast, for CBV80 the loss in BET surface area after steaming and reaction-regeneration cycles amounted to only 3%, which indicates that a major contribution in the loss of BET surface area of the extrudates (11%) can be attributed to the binder.

With respect to the pore characterization of the HZSM-5 extrudate after desilication, it has to be stated that the presence of an additional porous binder obviously complicates a detailed assessment of the porosity development in the zeolite crystal. Compared to the isotherm of the parent HZSM-5

extrudate, leaching with 0.3M NaOH led to a downward shift of the isotherm, caused by the loss in microporous material. Besides the ~40% decrease in V_{micro} from 0.11 to 0.07 cc/g, an increase in V_{meso} by ~20% resulted after the alkaline treatment with 0.3M NaOH. With increased leaching strength (0.5M NaOH), the loss in micropore volume was more severe and V_{micro} decreased to 0.04 cc/g.

Interestingly, the effect of steaming and repeated reaction-regeneration cycles on the pore structure was less pronounced for the mesoporous HZSM-5 extrudate compared to the parent HZSM-5 extrudates as the BET surface area decreased only by 2% (compared to 11% for Extr).

Groen et al. [28] reported a distinct increase in mesopore surface area from 120 to 180 m^2/g upon leaching of HZSM-5/alumina extrudates, whereas V_{micro} decreased from 0.12 to 0.08 cm^3/g. A similar decrease of ~30 % in V_{micro} was observed after the alkaline treatment of the corresponding zeolite powder.

TEM imaging of the mesoporous HZSM-5 extrudate (see Figure S5) confirms the creation of mesopores in the zeolite crystals (center of Figure S5), which reduces the size of the purely microporous domains. The less structured lumps shown at the top left corner and bottom of the image are attributed to the binder phase.

Chemical properties. With respect to the acidity of the catalysts, a clear drop (20–40%) in acidity was observed after the steam treatment for catalysts containing HZSM-5 (see **Table 2**). The subsequent reaction-regeneration cycles induced no or little (~1.5%) decrease of the zeolite's acidity, with the exception of the HZSM-5 extrudate for witch an additional drop by 12% was observed. While there are clear differences in the distribution of the acid strength, the total acidity of the equilibrated catalysts after steaming and use are rather close in the range 0.31–0.39 mmol NH_3/g. In order to quantify the Brønsted acidity, ethylamine was adsorbed from the vapor phase

onto a Brønsted acid site, where a proton transfer occurs. The alkylamine then decomposed to ethylene and ammonia through a Brønsted acid catalyzed Hoffman elimination reaction[38]. The numbers of Brønsted acid sites was then determined from the released ammonia, see **Table 2**. For the steamed versions of the parent HZSM-5, the parent HZSM-5 extrudate, and the parent mesoporous HZSM-5 extrudate quite similar Brønsted acidity remains. As such, neither the introduction of the binder phase nor the additional treatment of desilication and acid wash appear to have negatively influenced the steam-stability of the Brønsted acid sites. The Al_2O_3 binder phase itself contains 0.06 mmol NH_3/g Brønsted acidity. In contrast to HZSM-5 containing catalysts, Al_2O_3 maintains its total acidity, which amounts to 0.301 NH_3/g for the fresh catalyst and 0.308 mmol NH_3/g after steaming and three reaction/regeneration cycles, thereby indicating good hydrothermal stability.

For the mesoporous HZSM-5 extrudate, it should be kept in mind that the relative content of the binder phase was enhanced by the alkaline treatment. The parent extrudate was comprised of 65% HZSM-5 and 35% binder. Assuming that the ~10% mass loss by the desilication treatment can be solely attributed to the dissolution of the zeolitic phase, the resulting mesoporous HZSM-5 extrudate is comprised of 61% zeolite and 39% binder.

Table S1 (ESI) shows the comparison of elemental composition in terms of Si and Al content, as well as the Ca, Mg, K and Na content for selected catalysts after repeated use and regeneration. The hot gas filtration (350 °C) prevented the contact of ash-rich char particles with the catalyst and therefore the poisoning of the acid sites by the alkalines present in the wheat straw feedstock (1 wt-% K).

Product distribution. Figure 2 and Table S2 provide an overview of the product distributions (yields of dry, ash-free biomass). Results for SiC (grey bars) are included as non-catalytic

reference. Since results are shown on daf basis, the reaction water excludes the moisture in the biomass. It should be noted that the experiments obtained using SiC and the conventional HZSM-5 (Z801 to Z804) have recently been reported in our work testing the performance of desilicated HZSM-5 (Ref Fuel Proc. Tech. manuscript).

All catalysts were tested at 500 °C. In addition, runs were conducted with Al_2O_3 and desilicated HZSM-5/Al_2O_3 at a lower temperature of 450 °C, and an additional run was conducted with desilicated HZSM-5/Al_2O_3 at 550 °C (see legend of **Figure 2**). The char yields were in the range of 17–21 wt-% on daf basis and the fluctuations are attributed to the collection process. Hydrogen yields were negligible on a mass basis. In **Figure 2**, the C_4+ compounds analyzed in the gas phase are shown along the organic liquid (OL) yield, as they are expected to be condensed in full-scale processes at less diluted concentrations. The organic liquid comprises both the organics recovered as phase separated oil fractions and the organics in the aqueous fractions. While only the condensed liquid was analyzed, the addition of the mostly deoxygenated C_4+ compounds to the condensed oil is expected to further improve the oil properties, particularly its viscosity and evaporation behavior. For both the extrudates and its two constituents, with increased feeding of pyrolysis vapors the yields of gas, reaction water, and coke decreased while the OL yield increased. The lower gas yield observed with CBV80 at B:C = 9.9 compared to B:C = 17 likely resulted from an increased uncertainty in gas analysis at shorter runtimes. At the lower catalyst loadings, the gas concentration peaked within the first 5–10 min of operation after which it rapidly declined. Due to the gas sampling interval of ~13 min, the maximum gas concentration may have been missed in this case, which led to the calculation of an ~2.6 wt-% lower gas yield than would have resulted by monitoring of the gas concentrations with higher resolution.

Even for small amounts of catalyst (~25 g) and operation to B:C ratios >10, the OL yield obtained using SiC (500 °C) was not yet approached. For the Al_2O_3 binder, but also for the HZSM-5 extrudates a drastically reduced oil yield resulted when operated at low B:C, while the coke yield was markedly enhanced. Passing the vapors over Al_2O_3 at 450 °C (to B:C 6.2) instead of 500 °C (to B:C 7.3) led to a decrease in gas, reaction water and coke yield, while enhancing the OL yield (incl. C_4+) from 19 to 24%.

The product distribution obtained with mesoporous HZSM-5 extrudates operated at 500 °C and B:C = 2.1, 6.1 and 10.6 demonstrates the shift in product yields with increasing B:C ratio. In addition, the product distribution obtained at 500 °C and B:C ~6 was compared to runs at catalyst temperatures of 450 and 550 °C at similar B:C, respectively. Comparing the product distribution obtained with 260 g of the parent extrudates at B:C = 5.6 and 140 g of mesoExtr at 500 °C, indicates similar yields of CO, CO_2, and water. However, the mesoExtr yielded significant less olefins and C_1–C_3 gas products and about twice the amount of condensed OL. The slightly higher coke yield of the extrudates (4.2 wt-%) compared to the mesoExtr (3.5 wt-%) can be explained by the higher amount of extrudates loaded (260 g vs 140 g) and the slightly lower B:C ratio (5.6 vs 6.1). Table S3 provides a comparison of the carbon deposits of coke per surface area (micro- and mesopores) of the different catalysts and the comparison based on surface area shows that the coke deposits per surface area of the desilicated extrudates increased compared to its parent version when compared at similar catalyst volume and B:C ratio.

The variation in catalyst temperature between 450 and 550 °C strongly impacts the yield of gas, oil, and coke. The increased gas production at increasing temperature results mainly from enhanced CO and CO_2 yields, (Figure S6, ESI). The operation at a lower catalyst temperature of

450 °C improves the organic liquid yields and leads to reduced coke formation, while operation at 550 °C leads to a drastic decrease in oil yield to <13 wt-% (incl C_{4+}).

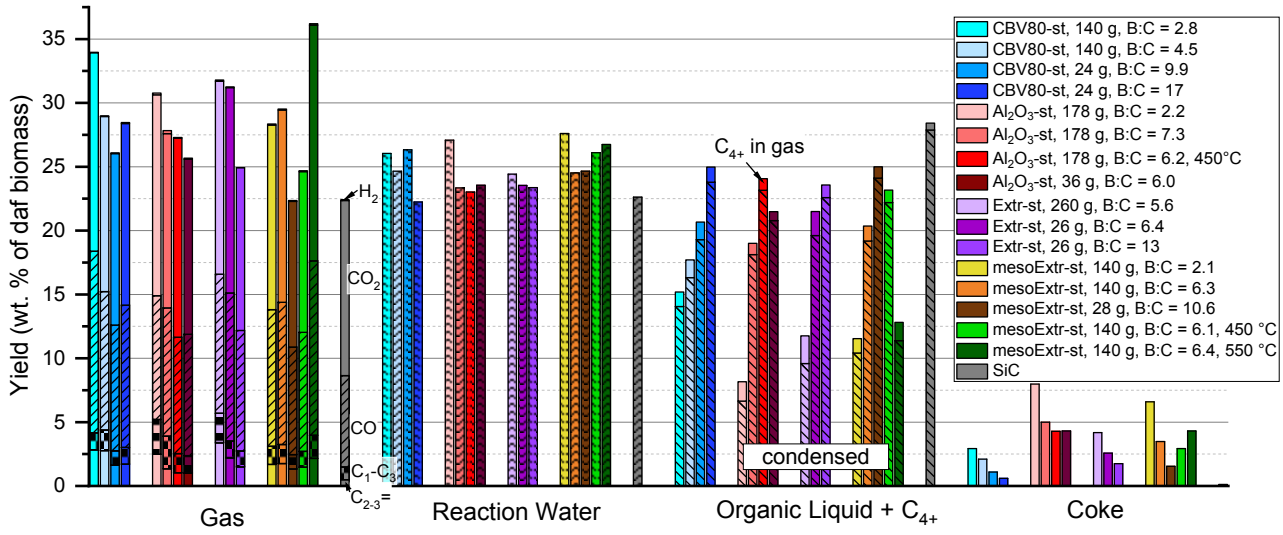

Figure 2. Product yields based on daf biomass when passing increasing amounts of wheat straw pyrolysis vapors over steamed HZSM-5 (CBV80-st), steamed alumina-binder (Al_2O_3-st), steamed HZSM-5 extrudates (Extr-st), and steamed mesoporous HZSM-5 extrudate (mesoExtr-st). Process conditions according to Table 1. Catalyst temperatures were 500 °C except when noted otherwise in the figure legend. The char yields were in the range of 17–21 wt-% (daf).

Liquid properties. The comparison of the oil quality focuses on the properties of the phase separated oil fraction and the carbon losses to the aqueous phase. Table S4 (ESI) summarizes the characterization of the non-catalytic reference oil obtained when vapors were passed over a SiC bed. Tables S3–S7 (ESI) summarize the properties of the obtained liquids using HZSM-5 as catalyst (experiments Z801 to Z804), Tables S6–S10 (ESI) summarize the properties of the obtained liquids using alumina as catalyst (experiments A801 to A804), Tables S11–S14 (ESI) summarize the properties of the obtained liquids using HZSM-5 extrudates as catalyst (experiments AZ801 to AZ804), and Tables S15–S19 (ESI) summarize the properties of the

obtained liquids using mesoporous HZSM-5 extrudates as catalyst (experiments mAZ801 to mAZ805). As indicated by the comparison of the organics distribution between the oil and aqueous phases in Table S5–S21, a higher fraction of the produced organics was recovered in the water fraction (mix WF) towards less severe deoxygenation. This holds true both for liquids collected at increased B:C ratios and at reduced catalyst temperatures.

Along with the oils' yield, moisture- and oxygen content (wt-% d.b.), **Table 3** provides an overview of the oils' total acid content and char remains upon TGA simulated distillation, with both the solid remains of the dry organics content at 300 °C and 500 °C indicated. The weight loss curves during TGA simulated distillation are provided in Figure S7–S10 (ESI). The TAN refers to the "wet" oil samples, i.e. the oil fraction including the dissolved water. While all four catalysts could reduce the oils' oxygen content below 10 wt-% d.b. at low B.C ratios, for oils collected at higher B:C ratios the oxygen content increased as result of catalyst deactivation (coking). The charring tendency positively correlates with the oxygen content of the oils, as shown in Figure S11 (ESI) for the mass remains of organics (d.b.) when heated to 200, 300, and 500 °C of all oils obtained using catalyst at 500 °C. A higher catalyst loading therefore leads to higher vapor conversion and oil with lower oxygen content, but the higher loading itself does not lead to substantially reduced charring. For mesoporous ZSM-5 extrudate, the effect of catalyst temperature on the charring tendency of the oils was moderate, as the mass remaining when heated to 300 and 500 °C was quite close for oils collected at catalyst temperatures of 450, 500 and 550 °C, even though the oils' oxygen and TAN decreased towards higher catalyst temperature. For alumina, a reduction in catalyst temperature to 450 °C at B:C ~6 increased the oil yield by ~20% to 16.8 wt-% of daf biomass; however, the oil's oxygen and TAN increased from ~12 to 21 wt-% (d.b.) and from ~17 to ~40 mg KOH/g, respectively. Even though the charring tendency increased,

the use of 1/5th of catalyst at 500 °C appears to reduce the oils' oxygen and TAN more efficiently compared to utilizing five times more catalyst at a lower temperature of 450 °C. Analysis of the derivative curves of the oils' weight changes upon heating (see Figure S10, ESI) indicates four distinct weight losses at 80, 116, 220 and 332 °C for the SiC oil. The weight loss above 300 °C may be attributed to thermal decomposition of residue[37]. For catalytically upgraded oils using mesoporous HZSM-5 extrudate, the weight loss at temperatures >300 °C was less distinct and the weight losses at ~80 °C and 200 °C were enhanced (see Fig. S10). The weight loss observed around 180–220 °C may be related to vaporization of (methoxy-)phenolics[39]. For the severely deoxygenated oil (B:C = 2.1, 6.3 wt-% O), the weight loss was most pronounced at ~100 °C, which could be attributed to vaporization of volatile non-polar compounds such as aromatic hydrocarbons[39]. This is in accordance with a higher volatility as the oils collected at low B:C ratio comprise a higher fraction of oil collected at the final condensation stage (−60 °C), which was more amenable for quantification by GC-MS/FID.

Table 3. Overview of oil properties for runs according to **Table 1**. Yield and C recovery of phase separated oil fraction (not including C_4+ measured in gas), moisture, oxygen content (d.b.), TAN, and mass fraction remaining with respect to dry organics content upon heating to 500 °C in a TGA (Pt crucible with lid, 10 °C/min heating rate, 150 ml/min flowrate N_2). Sulphur analysis according to ASTM method D5453. Catalyst temperature was 500 °C unless noted otherwise. Samples marked with an asterix (*) denote the use of less catalyst corresponding to 24-36 g (~60 ml).

Catalyst	B:C	Yield [wt-% of daf feed]	C recovery [wt-%]	H_2O [%]	wt-% O (d.b.)	TAN [mg KOH/g]	Solid remains [wt-% d.b.] at 300 °C/500 °C	Sulfur [wt-% d.b.]
SiC	11.0	19.4	29.2	14.7	21.4	54.4	44.5 / 16.9	0.07
CBV80-st	2.8	13.0	22.1	1.8	9.2	5.9	25.5 / 10.3	0.17
CBV80-st	4.5	14.5	23.9	3.1	13.6	7.8	27.2 / 10.5	0.12
CBV80-st*	9.9	16.6	26.2	4.1	16.0	18.5	42.7 /17.6	n.d.
CBV80-st*	17	19.1	29.0	3.4	20.2	23.6	45.2 /18.4	n.d.
Alumina-st	2.2	5.7	10.5	4.5	2.7	1.3	20.1 / 4.4	0.30
Alumina-st	7.3	14.0	23.1	2.7	11.8	17.2	23.1 / 9.4	0.22
Alumina-st (450 °C)	6.2	16.8	25.0	3.7	21.0	40.2	26.6 / 10.2	n.d.
Alumina-st*	6.0	15.6	25.0	3.2	14.5	34.8	32.4 / 12.7	n.d.
Extr-st	5.6	7.7	13.5	2.0	7.7	<3.4	17.4 / 5.7	0.14
Extr-st*	6.4	14.8	23.4	2.8	15.5	18.7	28.5 / 11.7	n.d.
Extr-st*	13	17.3	26.7	3.8	17.4	22.6	33.9 / 15.1	n.d.
mesoExtr-st	2.1	9.7	17.0	1.8	6.3	6.5	18.9 / 5.2	0.22
mesoExtr-st (450°C)	6.1	18.0	26.9	4.1	19.1	37.4	24.2 / 11.9	0.09
mesoExtr-st	6.3	15.5	24.2	2.6	17	12.5	25.1 / 11.1	0.22
mesoExtr-st (550 °C)	6.4	11.4	19.1	2.6	10.8	4.0	25.5 / 11.3	n.d.
mesoExtr-st*	10.6	19.5	29.3	4.5	19.8	34.8	30.3 / 15.6	n.d.

With increased deoxygenation the sulfur (S) content in the oil increased, both for the oils obtained using the zeolite containing catalysts but also for the alumina binder itself (**Table 3**). The maximum increase in S was observed for oil obtained from alumina at B:C = 2.2, where the

severely deoxygenated oil (2.7% O) showed 0.3 wt-% S compared to 0.07 wt-% S of the SiC oil. While the nature of the condensed S species was not investigated in this study, we note that the formation of S impurities in gasoline obtained from fluid catalytic cracking was attributed to the reaction of H_2S with olefins or diolefins to form alkylthiophenes[40]. An increased deoxygenation severity increased the yield of olefins not only for HZSM-5 containing catalysts but also for Al_2O_3. The observed shift to lower MW and a decrease in oil yield indicates that the increased S content can be attributed to higher concentration of low MW S-containing compounds. Depending on the oil's application, the sulfur and nitrogen constituents can be suitably removed by hydrotreating.

Size exclusion chromatograms (SEC) for oils obtained with CBV80, Al_2O_3, HZSM-5 extrudates, and desilicated HZSM-5 extrudate are compared in **Figure 3**. For chemically analogous compounds, a higher retention volume indicates a shift to lower molecular weight. The negative peak at 10.4 ml is most probably due to the presence of water in the samples. There are at least seven discernable components in the SEC trace for SiC oil. Based on the elution of a dodecastyrene standard with MW = 1250 Da at 7.57 mL, the compounds of the derived oils appear to have a MW below ~1000 Da. Compared to the SiC oil, the catalytically obtained oils, have reduced contributions of high MW compounds and a more intense differential refractive index (DRI) output of low MW compounds eluting at 9.7 mL, especially for oils collected at low B:C ratio and higher temperature (550 °C) (see **Figure 3**). For oils collected at higher B:C ratio or lower temperature (450 °C), this low MW response decreased and contributions of higher MW compounds eluting below 9.25 mL increased to levels similar to the SiC oil. The low MW response remained enhanced compared to the SiC oil even for catalytically obtained oils at high B:C ratios. Oil obtained using 36 g Al_2O_3 at B:C = 6 and oil obtained using an about five times higher amount of catalyst at similar B:C ratio but lower temperature of 450 °C showed quite similar MW distribution. The

484 results indicate that a breakdown of the primary bulky pyrolysis vapors into low MW compounds
485 occurred more effectively at low B:C ratio; however, it can also be achieved for oils collected at
486 higher B:C ratio and elevated catalyst temperature.

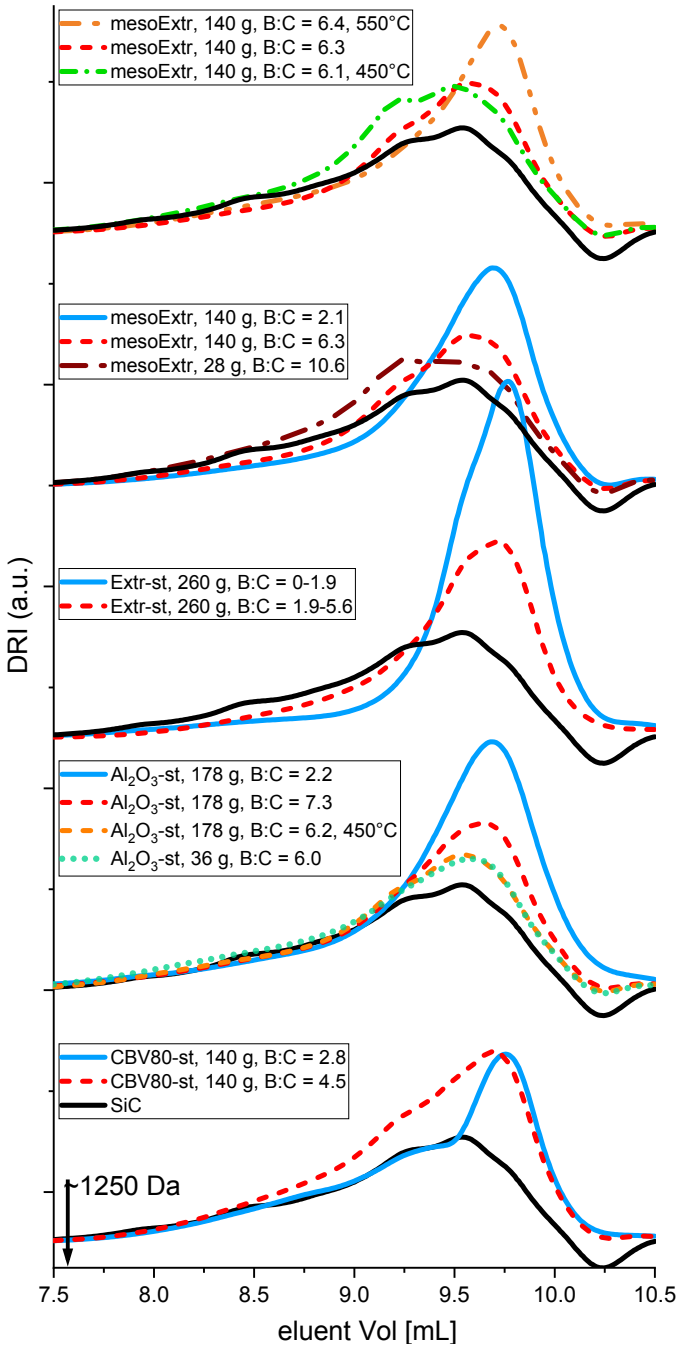

487

488 **Figure 3.** SEC chromatograms for oils obtained using CBV80, alumina, HZSM-5 extrudates and
489 mesoporous HZSM-5 extrudates as catalyst.

The quality of the derived oils at 500 °C can be compared by plotting the molar H/C ratio against the molar O/C ratio (see **Figure 4**). The number next to each data point indicates the yield of the oil fraction (not including organics in WF and C_4+). The O/C ratio was clearly reduced by using a larger amount of catalyst and stopping the experiments at low B:C ratio. This resulted in decreased H/C ratios due to the favored dehydration pathway at low B:C. Amongst the different catalysts, oils obtained from Al_2O_3 showed the highest H/C ratios. The extension of the H/C ratios towards complete deoxygenation for the HZSM-5 and HZSM-5 extrudate oils approaches H/C ~1, in agreement with the enhanced aromaticity observed by GC-MS/FID and NMR characterization (vide infra). When extrapolating the trends of the H/C ratio obtained with higher amounts of catalyst towards higher O/C ratios, the results obtained using reduced amounts of catalyst fall below those extrapolations. This could be related to the reduced coking rate at lower catalyst loadings, resulting in reduced incorporation of hydrogen into vapor compounds during the formation of carbon-rich coke. The trend observed for the H/C ratios in the oils correlates with the coking tendency. As such, it cannot be excluded that the higher coking rates observed for Al_2O_3 and HZSM-5/Al_2O_3 allowed more hydrogen to be incorporated into the vapors.

Dehydration appears to be favored mainly at low B:C ratio by the Brønsted acidity, while oxygen removal in the form of CO_x prevails once the Brønsted acid sites are poisoned by coke and only weak acid sites—presumably of the Lewis type—remain (see NH_3-TPD of coked HZSM-5 extrudate after B:C = 5.6 in Figure S3, ESI). Figure S12, ESI, shows the effect of the catalyst temperature on the molar H/C and O/C ratios of the obtained oils using Al_2O_3 and mesoExtr. A reduction in catalyst temperature from 500 to 450 °C for Al_2O_3 resulted in a slight reduction in H/C ratio, but a clear increase in O/C ratio from 0.12 to 0.23, close to the SiC oil (O/C = 0.24). Decreasing the temperature from 550 °C to 500 °C and 450 °C for the hierarchical HZSM-5

extrudate gradually increased the O/C ratio. At 450 °C, the mesoExtr-st achieved a 1.2 wt-% higher oil yield compared to Al_2O_3 at a lower O/C ratio (Figure S12). Within the investigated temperature range, the Al_2O_3 derived oils show higher H/C ratios compared to the mesoporous HZSM-5 extrudate, which may result from the higher coking propensity of Al_2O_3 and/or the higher dehydration activity of HZSM-5 containing catalyst.

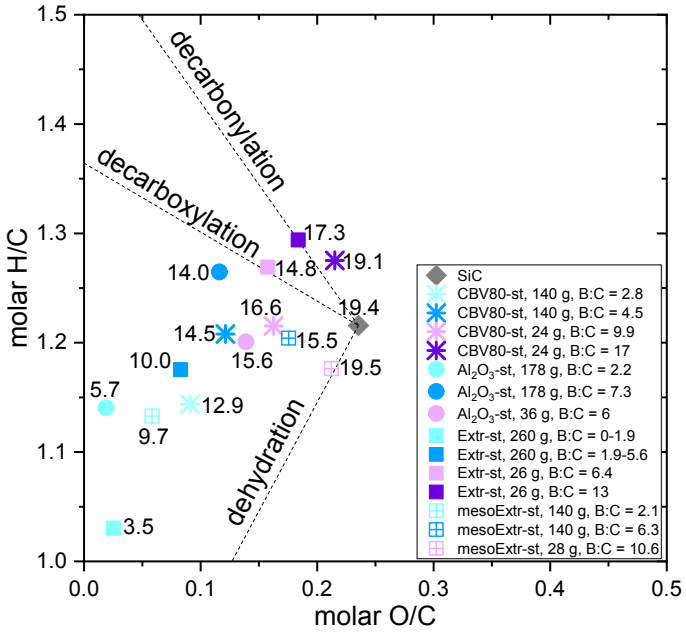

Figure 4. Molar H/C ratio and O/C ratio for the phase separated oil fractions obtained using CBV80, alumina, HZSM-5 extrudates and mesoporous HZSM-5 extrudates (all steamed) as catalyst at 500 °C. Oil obtained with empty catalytic reactor and SiC shown for reference. Numbers next to symbol indicate the oil yield (wt-% of daf biomass).

The yield of compounds in the liquid products obtained from CBV80, alumina, and HZSM-5 extrudates as catalyst is shown in **Figure 5** and will be discussed separately for the oil and aqueous fractions. Liquids obtained using a larger amount of catalyst (~300 mL) are indicated by 'L', whereas liquid products obtained using less catalyst (~60 mL) are indicated with 'S'. Clearly

enhanced monoaromatics yields of 2.3 wt-% (of daf straw) resulted using 140 g of CBV80 at B:C = 2.8; however, the monoaromatics yields rapidly decreased as seen by a yield of 1.7 wt-% at B:C = 4.5. A significant drop in monoaromatics yield resulted when using less catalyst at B:C = 9.9 and an increase in oxygenates, especially methoxy-phenols, acids, alcohols, aldehydes and ketones was observed. For the oil fractions obtained from Al_2O_3, the monoaromatics yields were not particularly enhanced at larger catalyst mass. No acids were observed for oils collected at B:C = 2.2 and 7.3 at 500 °C using 178 g of alumina; however, acids appeared in the product slate when loading less catalyst or lowering the temperature to 450 °C at B:C ~6. Not surprisingly, the monoaromatics yields were enhanced over the HZSM-5 extrudate compared to alumina, however at lower yields compared to the runs with HZSM-5 only, in agreement with Zhang et al.'s [41] observations when physically mixing HZSM-5 with γ-Al_2O_3 in equal proportions. While the yield of monoaromatics decreased towards increased B:C ratio and by using less catalyst, it is interesting to note the pronounced selectivity towards phenols, especially over the partly coked extrudate (B:C = 1.9–5.6) resulting in a yield of 1.8 wt-%. This suggests that besides the phenols resulting from cracking of lignin-derived primary vapors, they may constitute intermediate products of catalytic origin[42–45]. Comparing the results at lower catalyst loadings, the yield of phenols was about 30% higher using the Al_2O_3 and HZSM-5 extrudate at B:C ~6 compared to the results obtained with HZSM-5 only. The breakthrough of oxygenates and decrease of aromatic yields with increasing B:C ratios for HZSM-5/Al_2O_3 extrudates agrees with work reported by Murillo et al.[14]. The selectivity within the obtained monoaromatics to benzene, toluene, and xylenes (BTX), alkyl and alkenyl-benzenes, as well as indenes is provided in Figure S13, ESI. In accordance with the trends observed for the monoaromatics yields, the BTX selectivity was highest for CBV80 and the HZSM-5 extrudate, while Al_2O_3 has a high selectivity to alkylated benzenes.

In the phase separated oil fraction obtained with mesoporous HZSM-5 extrudate as catalyst (**Figure 5**a), a clear enhancement of monoaromatics and phenols was observed compared to SiC. The yield of monoaromatics and phenols decreased towards higher B:C ratios and reduction in catalyst temperature, along with a breakthrough of methoxy-phenols, acids, ketones, and aldehydes. The results indicate that conducting the catalytic vapor treatment at 550 °C allows to obtain a similar yield of valuable products at B:C ~6 compared to operating at B:C ~2 and 500 °C, thereby reducing the regeneration frequency by ~2/3. The selectivity within the obtained monoaromatics to BTX, alkyl and alkenyl-benzenes, as well as indenes when using mesoporous HZSM-5 extrudate is shown in Figure S14. Overall, the BTX selectivity followed the trend of the monoaromatic yields, i.e. with increasing catalyst deactivation at high B:C or at moderate temperature (450 °C), the BTX selectivity decreased. While the selectivity to benzene was little affected, the changes for toluene and p-xylene were more pronounced.

Acids, aldehydes and ketones are the main product groups found in the WF due to their polar nature and water-solubility (**Figure 5**b). At low B:C, the yield of these oxygenates was reduced due to their effective cracking. At low B:C ~2 and at elevated temperature of 550 °C, increased yields of phenols were recovered in the WF when using the conventional and desilicated HZSM-5/Al_2O_3 as catalyst. The yield of acids increased at lowered catalyst temperature and towards higher B:C ratio, indicating their less effective conversion at reduced catalyst activity. The yield of acids recovered in the aqueous phase positively correlated with the TAN of the oil phase (see **Table 3** and Figure S15a). The higher moisture content and polarity of the less deoxygenated oils likely facilitated the solvation of acids. At 550 °C, acids could be removed very efficiently, which agrees with the clear reduction in TAN from ~37 mg KOH/g at 450 °C to ~4 mg KOH/g at 550 °C for oils collected at B:C ~6 using desilicated HZSM-5/Al_2O_3 (see **Table 3**). While aldehydes

appeared less affected by variations in B:C ratio or temperature, ketones followed the same trend as acids. Elevated yields of methoxy-phenols and (anhydro)sugars were recovered in the aqueous fraction obtained from SiC. These groups can be attributed to primary pyrolysis vapors from the thermal breakdown of lignin and cellulose, respectively.

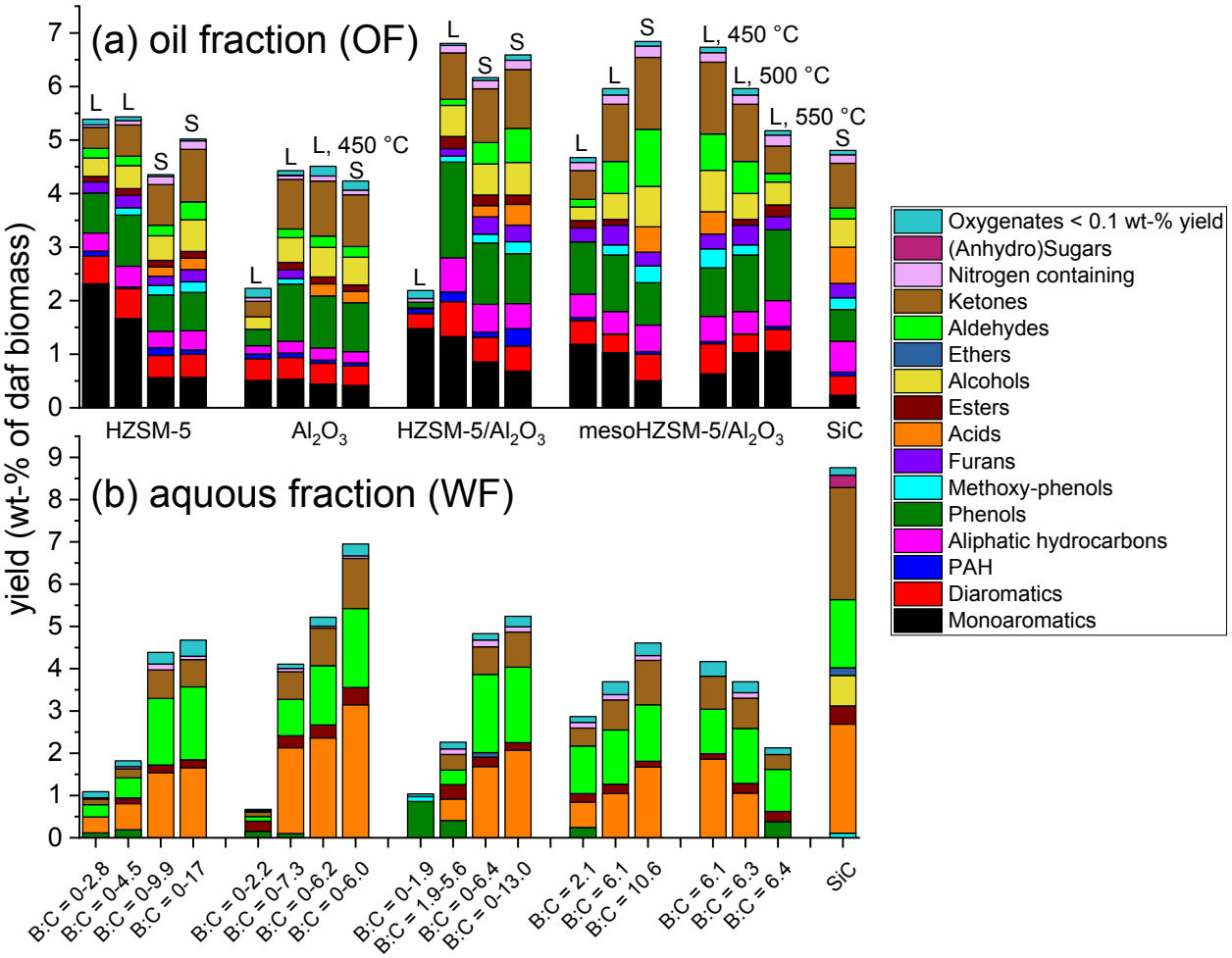

Figure 5. Yields of GC identifiable products for oils obtained using HZSM-5 (CBV80), Al_2O_3, HZSM-5/Al_2O_3, and mesoporous HZSM-5/ Al_2O_3 extrudate as catalysts (all steamed). **Figure 5**a shows the yields recovered in the oil fraction (sum OF), while **Figure 5**b shows yields recovered in the aqueous fraction (sum WF). Liquids obtained using a larger amount of catalyst (~300 mL) are indicated by 'L', whereas liquid products obtained using less catalyst (~60 mL) are indicated

with 'S'. Annotations in top graph applies for both graphs. Amounts of catalyst used and reaction conditions according to **Table 1**.

While GC-MS/FID analysis allowed a detailed analysis of the chemical composition, it only identified a fraction of the oil since up to 50% of the oils' mass may remain upon heating to 250 °C at the injection, as seen from evaporation in a TGA (see Figure S7–S10). In order to analyze the chemical composition of the whole oils, selected oils were subjected to ^{1}H, ^{13}C NMR and 2D HSCQ NMR analysis. Figure S16 and S17 (ESI) show a comparison of the processed ^{1}H NMR spectra. The relative distribution of the different chemical groups was obtained by assigning the functional groups to their chemical shift ranges and excluding the peak area contributions of water (3.7–3.3 ppm) and the DMSO solvent (2.5 ppm). The H percentages are summarized in **Table 4**, with the assigned protons marked underlined. Acid groups are not reliably quantified by ^{1}H NMR due to rapid proton exchange with residual water present in the oil and solvent. Compared to the SiC oil, the catalytically obtained oils show elevated H concentrations of the sum of –CHO and ArOH, in agreement with an enhanced phenol and/or aldehyde content measured within the GC-identifiable range. The H percentage within aromatics and conjugated alkenes increased from 12% (SiC) to 29% using CBV80 (B:C = 4.5). Even higher H percentage of aromatics and conjugated alkenes resulted using the HZSM-5 extrudate (B:C = 5.6) with 35.1%, and when using the mesoporous HZSM-5 extrudate at B:C = 2.1 (32.0%) or at elevated temperature of 550 °C at B:C = 6.4 (34.4%). Using Al_2O_3 or mesoporous HZSM-5 extrudate at reduced temperature of 450 °C leads to reduced aromaticity of the oils (~22–23% H). Protons bound in aliphatic O<u>H</u>, -C<u>H</u>=C<u>H</u>-, and Ar−C<u>H</u>$_2$-O−R amounted to 4.7% for the SiC oil and this contribution was clearly reduced by the use of all catalysts, yet less effectively at a temperature of 450 °C using the mesoporous HZSM-5 extrudate (3.7%) or Al_2O_3 (2.6%). For the H percentage of ether (R−C<u>H</u>$_2$−O-R) and methoxy

(C$\underline{H}_3$−O−R) groups, those contributions could be effectively reduced with Al_2O_3 at 500 °C, while at 450 °C using mesoExtr the relative H% of these groups closely approached the SiC oil. The relative H contribution of aliphatics (2–0 ppm) was most pronounced using the alumina binder (31.6%) compared to the SiC oil (24.6%).

^{13}C NMR analysis of the oils provides spectra with less overlap of chemical shifts compared to ^{1}H NMR. Figure S18 and S19 (ESI) show a comparison of the ^{13}C NMR spectra of the oils and **Table 5** summarizes the C percentage within a given chemical shift range. The assignment of chemical shift regions was conducted according to Mante et al.[46] and Joseph et al.[47]. The SiC oil showed a high amount of oxygenated compounds with carbonyl, carbohydrates and methoxy/hydroxyl containing groups constituting 27.6 C%. These fractions were effectively reduced to ~9–13 C% for the majority of the catalytically obtained oils that were analyzed by NMR, with the exception of the oil collected from Al_2O_3 (20.4 C%) and mesoporous HZSM-5 extrudate at 450 °C (22.4 C%). The C percentage of aromatics including olefins and phenolics increased for all catalysts compared to the SiC oil–yet more pronounced for HZSM-5, HZSM-5 extrudate, and the mesoporous HZSM-5 extrudate at B:C = 2.1 (500 °C) and B:C = 6.4 (550 °C), which can be attributed to the shape selectivity of the zeolite's micropores. The contribution of aromatics and olefins was clearly enhanced and the content of aliphatic hydrocarbons decreased when increasing the temperature from 450 °C to 550 °C using mesoporous HZSM-5 extrudate, while the temperature increase had little effect on the content of aromatic carbons in phenol and methoxylated phenols. Compared to the SiC oil, the C contribution of lignin derived methoxy-groups (57–55 ppm, 3.9 C%) was effectively reduced by all catalysts–however, least effectively at the reduced catalyst temperature (450 °C) using the mesoporous HZSM-5 extrudate.

Table 4. Hydrogen percentage based on the ^{1}H NMR analysis of the oils obtained from passing straw fast pyrolysis vapors over SiC, CBV80, HZSM-5 extrudate, alumina, and mesoporous HZSM-5 extrudate at the indicated B:C ratios. Catalyst temperature was 500 °C unless noted otherwise. The H% for oil from HZSM-5 extrudate at B:C = 5.6 has been calculated based on the oil yields and H% of oils collected at B:C = 0–1.9 and 1.9–5.6.

Assignment	Chemical shift range (ppm)	SiC	CBV80, B:C = 4.5	Extr, B:C = 5.6 (calc.)	Alumina, B:C = 7.3	mesoExtr, B:C = 2.1	mesoExtr, B:C = 6.1, 450 °C	mesoExtr, B:C = 6.3, 500 °C	mesoExtr, B:C = 6.4, 550 °C
-COO<u>H</u>	12.5–11.0	0.2%	0.1%	0.1%	0.2%	0.1%	0.2%	0.0%	0.1%
-C<u>H</u>O, ArO<u>H</u>	11–8.2	0.7%	2.9%	3.3%	2.2%	2.7%	2.0%	1.4%	1.4%
aromatics and conjugated alkene <u>H</u>	8.2–6	12.0%	29.2%	35.1%	22.1%	32.0%	22.7%	28.7%	34.4%
aliphatic O<u>H</u>, -C<u>H</u>=C<u>H</u>-, Ar−C<u>H</u>$_2$-O−R	6–4.2	4.7%	2.2%	1.1%	2.6%	2.0%	3.7%	3.4%	1.8%
R−C<u>H</u>$_2$−O-R, C<u>H</u>$_3$−O−R	4.2–3	9.6%	5.0%	2.1%	2.3%	1.3%	9.5%	5.8%	1.8%
aliphatic H, -C<u>H</u>R-C=O, -C<u>H</u>R-C=C	3.0–2.0	48.4%	39.6%	43.1%	39.0%	46.6%	33.3%	38.3%	48.0%
aliphatic <u>H</u>	2.0–0	24.6%	20.9%	15.3%	31.6%	15.3%	28.5%	22.5%	12.4%

Table 5. Carbon percentage based on the ^{13}C NMR analysis of the oils obtained from passing straw fast pyrolysis vapors over SiC, CBV80, HZSM-5 extrudate, alumina, and mesoporous HZSM-5 extrudate at the indicated B:C ratios. Catalyst temperature was 500 °C unless noted otherwise. The C% for oil from HZSM-5 extrudate at B:C = 5.6 has been calculated based on the oil yields and C% of oils collected at B:C = 0–1.9 and 1.9–5.6.

Assignment	Chemical shift range (ppm)	SiC	CBV80, B:C = 4.5	Extr, B:C = 5.6 (calc.)	Alumina, B:C = 7.3	mesoExtr, B:C = 2.1	mesoExtr, B:C = 6.1, 450 °C	mesoExtr, B:C = 6.3, 500 °C	mesoExtr, B:C = 6.4, 550 °C
aldehydes, ketones	220–180	7.8%	4.0%	4.1%	9.3%	5.1%	8.7%	6.2%	5.1%
CO groups (carboxylic acids and derivatives)	180–160	7.6%	2.6%	2.1%	4.6%	2.3%	6.1%	3.5%	3.0%
aromatic carbons in phenol	160–140	12.6%	10.8%	10.4%	10.4%	10.0%	13.1%	12.5%	12.0%
aromatics and olefins	140–125	9.1%	29.7%	33.4%	17.7%	31.3%	13.0%	18.1%	27.9%
methoxylated phenols (guaiacyl/syringyl)	125-105	14.2%	14.8%	15.4%	15.2%	14.9%	15.6%	18.6%	18.5%
levoglucosan, anhydrosugars, alcohols, ethers	105–60	8.3%	3.8%	2.7%	5.5%	3.4%	4.6%	6.0%	4.5%
methoxyl-group in lignin	57–55	3.9%	1.5%	0.4%	1.0%	0.6%	3.0%	1.7%	0.7%
aliphatic hydrocarbons	55–0	36.4%	32.8%	31.5%	36.4%	32.4%	36.0%	33.4%	28.3%

Comparison of coking propensity. For the freshly calcined zeolite, the initial rate of dealumination is high upon exposure to hydrothermal conditions[48]. When starting the vapor upgrading, the activity of the freshly calcined catalyst would therefore decrease both due to coke deposition and due to the simultaneous dealumination. Steaming prior to reaction, as was done in this study, allowed to better disentangle these two effects.

In order to compare the coking propensity of the HZSM-5 extrudate and its two constituents, the build-up of carbon as coke normalized by the amount of catalyst was plotted against increasing

amounts of pyrolysis vapors passed over the catalyst (in terms of increasing B:C ratios) (see **Figure 6**). Clearly, large differences in the coking propensity are observed and the increased coke deposition on the HZSM-5 extrudate compared to the pure zeolite can be attributed to the alumina binder, as previously observed[8,12,13]. About two to three times more coke was formed on the binder compared to the HZSM-5 itself when using ~300 mL catalyst volume. **Figure 6** also shows a clear effect of the catalyst loading on the coking propensity. While the extent of deoxygenation was more severe when utilizing larger amounts of catalyst, more coke deposited compared to the reduced catalyst loadings (~60 mL). Table S3 indicates a negative correlation of the deposited carbon per surface area and the catalyst surface area when comparing the results obtained at similar catalyst volume and B:C ratio. Since for HZSM-5 containing catalysts the micropores contribute the most to the total surface area, the results confirm that the micropores of HZSM-5 limit coke formation compared to alumina. The desilication leads to i) a decrease of the micropore surface area and an increase of the surface area of mesopores (see **Table 2**), and ii) a higher fraction of alumina in the desilicated HZSM-5/Al_2O_3 extrudates. Both aspects can contribute to the increased coking propensity of the latter.

A clear effect of temperature on the coking propensity was demonstrated using the mesoporous HZSM-5 extrudate (see Figure S20), with an increase from 0.178 to 0.274 g coke/g catalyst when increasing the temperature from 450 °C to 550 °C at B:C ~6.

Fig. S21 shows a comparison of the evolution of CO and CO_2 during the oxidative regeneration of coked catalyst when ramping the combustion temperature (1°C/min). It can be seen that the coke on Al_2O_3 combusted most easily and predominantly resulted in CO_2 formation, while coke on HZSM-5 required ~200 °C higher combustion temperatures. The coke on the parent HZSM-5/ Al_2O_3 combusted more readily compared to the HZSM-5, which is attributed to the Al_2O_3

component. Lower combustion temperature of combined char and coke on Al_2O_3-SiO_2 matrix and Al_2O_3 binder compared to HZSM-5 was also reported by Du et al.[13,49] after CFP of miscanthus in direct contact with the catalyst. For the desilicated HZSM-5/Al_2O_3, we find that the coke combusted more readily compared to the parent HZSM-5/Al_2O_3 (see Fig. S21).

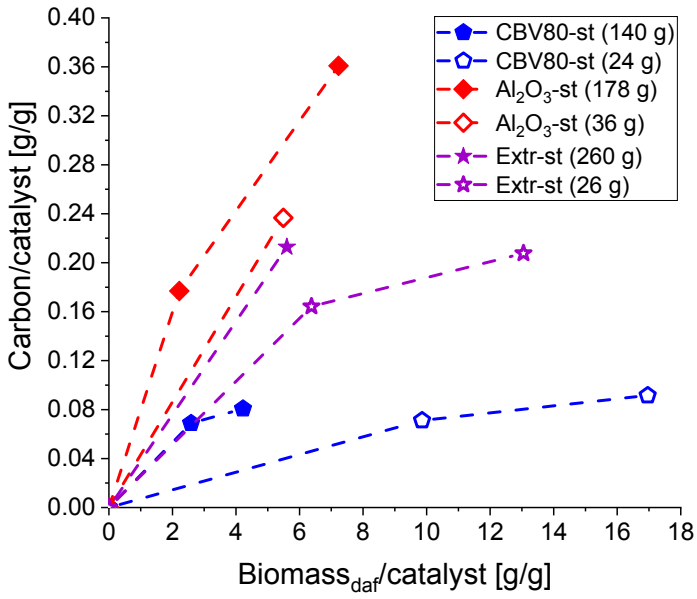

Figure 6. Build-up of carbon (as coke) on steamed HZSM-5 (CBV80-st), steamed alumina (Al_2O_3-st), and steamed HZSM-5/Al_2O_3 extrudates (Extr-st) shown for increasing B:C ratios and experimental conditions according to Table 1.

Process-performance. The energy distribution was calculated based on the mass yield of each product fraction and its heating value. The higher heating value (HHV) for the char and the oil fraction was calculated based on their elemental composition[50], and the HHV of the gas was calculated based on the HHV of the individual gas components. On daf basis, the char contained 2 wt-% N, 80 wt-% C, 4 wt-% H, and 14 wt-% O, corresponding to 31 MJ/kg. **Figure 7** shows a comparison of the energy balance for the different catalysts. Besides the thermal reference using a SiC bed, also the energy balance for an empty reactor was included. The sum of all condensable

organics (including C_4+) was highest for the empty reactor case, followed by SiC. For all four catalysts, with increasing B:C ratios the energy losses to gas and C_4+ decreased (see **Figure 7**), while the energy recovery of the organics recovered as oil phase increased. In comparison to the empty catalytic reactor, the use of SiC led to a reduction in the energy recovery of organic liquid and C_4+ from ~50% to ~44%. 'L' and 'S' in **Figure 7** indicate if a larger or smaller amount of catalyst was utilized. While the energy recovery of the aqueous fraction was not determined since no complete elemental analysis of the highly diluted organics was obtained, Fig. S22 and S23 show the carbon recovery of the aqueous phase. Increased losses of organics to the aqueous phase resulted towards higher B:C ratios or when less catalyst and a lower temperature was applied for the vapor upgrading. It is noteworthy that a quite similar energy balance resulted for Al_2O_3 at B:C = 6 when using 180 g catalyst at 450 °C compared to using only 40 g catalyst at 500 °C. The use of the Al_2O_3 binder or extrudate at low B:C ratio increased the carbon losses to coke and the energy recovery of the gas phase, at the expense of energy recovery as organic liquid. As an example, for Al_2O_3 at B:C = 2.2, the carbon recovery as condensed oil phase amounted to only 10.5%, which was less than the carbon lost as coke (17.2%).

Also for mesoporous HZSM-5 extrudates, the energy recovery as organic liquid and C_4+ improved with increasing B:C ratio from ~29% (B:C = 2.1) to ~40% (B:C = 10.6), while the energy recovery of the gas phase was reduced from ~17% to ~9%. When varying the temperature at B:C ~6, the energy recovery as NCG was clearly enhanced at 550 °C, while less carbon was lost to the aqueous phase (see Fig. S23). Higher temperatures thus favored the production of gas and bio-oil aromatics, however at reduced liquid yields. This is in agreement with results by Du et al.[13], who investigated the effect of temperature for CFP using HZSM-5.

The carbon product distribution from runs obtained with the zeolite, the binder, and the HZSM-5 extrudates is shown in Figure S22 (ESI). The C recovery of the condensed OF increased with increasing B:C ratio, and the C recovery of the SiC reference oil (29.2 wt-%) was closely approached for B:C = 17 using CBV80-st. C_4+ products tend to decrease with increasing B:C, along with decreasing C losses to NCG but increasing losses to the WF. The aqueous fraction from the SiC run contained >10% of the biomass carbon whereas for the majority of the catalytic runs less than 5% carbon were lost to the aqueous phase (at low B:C ratio even less than 2.5%). For the Al_2O_3 binder, the carbon losses to the aqueous phase clearly increased at a lower catalyst temperature of 450 °C compared to 500 °C. It is interesting to note that a nearly identical C product distribution at B:C = 6 was obtained with 36 g Al_2O_3 operated at 500 °C compared to the five times higher amount (178 g) operated at B:C = 6.2 and 450 °C, in agreement with the similar energy recovery, monoaromatics selectivity, and MW distribution. Carbon losses to coke are highest for the alumina binder and lowest for the HZSM-5. Severe deoxygenation at low B:C using the Al_2O_3 itself thus appears unfavorable due to >15 wt-% carbon losses to coke.

Likewise, for the mesoporous extrudates (Figure S23, ESI) an increased C recovery of the condensed oil fraction but also increased losses to the aqueous phase resulted towards higher B:C ratios, while the losses to C_4+, NCG, and coke decreased. Comparing the effect of temperature at a B:C ratio of ~6 shows that by lowering the catalyst temperature the product distribution changed in the direction as it would for higher B:C ratios and reduced catalyst activity/amount. An increase in catalyst temperature to 550 °C at B:C ~6 led to a product distribution similar to that obtained at B:C ~2 and 500 °C. Even though the NCG yield was markedly higher at 550 °C and B:C ~6 compared to B:C~2 at 500 °C, a higher carbon and energy recovery of oil phase resulted for the

former, 19.1 wt-% carbon/20.3% energy recovery, compared to 17 wt-% carbon/18.4% energy recovery for the latter, which is in line with the high losses of carbon to coke at low B:C ratio.

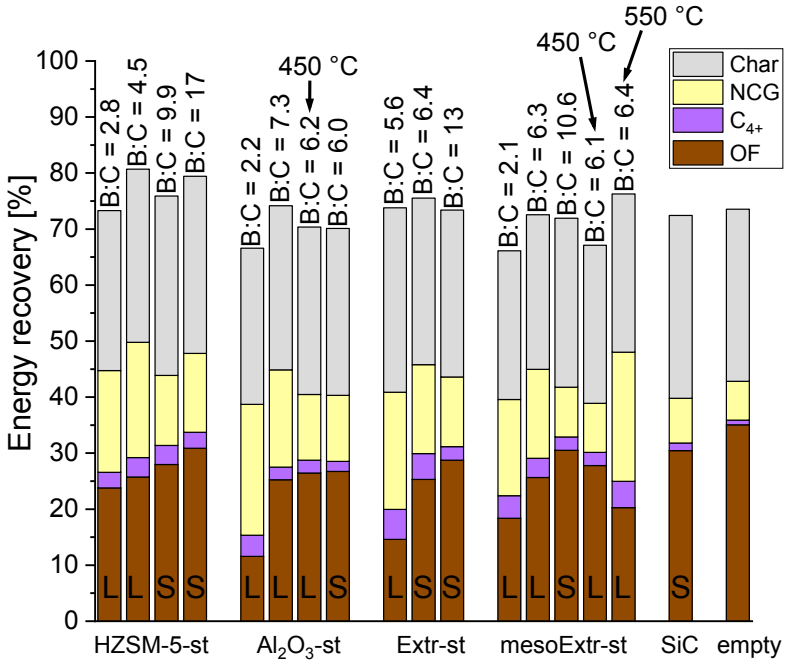

Figure 7. Energy recovery of phase separated oil fraction, C_4+, non-condensable gases, and char when upgrading wheat straw FP vapors with steamed CBV80, Al_2O_3, HZSM-5/Al_2O_3 extrudates, and mesoporous HZSM-5/Al_2O_3 extrudates as catalyst. Energy recovery of aqueous stream and coke not shown (please see Fig. S22 and S23 for carbon recovery). Catalyst temperature was 500 °C unless noted otherwise. Energy balance for empty catalytic reactor and SiC at 500 °C shown for reference. 'L' and 'S' indicate if a larger (~300 mL) or smaller (~60 mL) amount of catalyst was employed.

Discussion

The organics recovered in the aqueous fraction have to be separated by further processing steps and the aqueous phase as such does not have an application as fuel but may be considered waste water. As such, it is desirable to limit the loss of organics to the aqueous phase. It can be seen from Fig. S22 and S23 that for all catalysts the carbon recovery of the WF was lower compared to the

SiC case. An increase in catalyst temperature clearly enhanced the activity and a 5 times lower amount of catalyst at 500 °C compared to at 450 °C achieved the same degree of deoxygenation, as was demonstrated using Al_2O_3 and mesoporous HZSM-5/Al_2O_3 extrudates as catalysts. Du et al. [49] investigated catalytic pyrolysis of miscanthus over HZSM-5 in the temperature range of 400–600 °C and B:C ratios ≤1 (in situ spouted bed), and concluded that the selectivity to aromatics increased with temperature, which is in agreement with our results. Puertolas et al.[52] reported a positive correlation between the yields of CO and aromatics. As seen in Figure S6, the yields of CO, CO_2, and C_{2-3} olefins increased exponentially with temperature, while the yields of C_{1-3} alkanes and C_4+ increased linearly. A positive correlation between CO and aromatics yield (see **Figure 5** and **Table 4-5**) is therefore in line with observations by Puertolas et al.[52].

The increased coking with HZSM-5/Al_2O_3 compared to pure HZSM-5 is consistent with several studies attributing high coke yields to alumina, which is likely due to its high content of mesopores[15,19,49].

A comparison of the extent of deoxygenation (relative to the SiC oil, 21.5 wt-% O (d.b.)) and the carbon recovery in the phase separated oil fraction is shown in **Figure 8**a. While there are some differences between the different catalysts tested, it is interesting that at 500 °C the trend is consistent for all catalysts that with increase in deoxygenation severity, the carbon recovery in the oil phase decreased (due to higher losses to coke, NCG and C_4+). While a decrease in catalyst temperature to 450 °C led to a pronounced decrease in deoxygenation activity for Al_2O_3 (from 11.8 wt. % O in the oil to 21.0 wt. % O in the oil) the decrease in deoxygenation activity for mesoporous HZSM-5 extrudates at 450 °C compared to 500 °C was less pronounced (from 17.0 wt. % O in the oil to 19.1 wt. % O in the oil). A slightly different picture is obtained when comparing the deoxygenation and energy recovery of the condensable vapors, that is the sum of

organic liquid (OF + WF) and C_4+, relative to the results obtained with an empty reactor (see **Figure 8**b), which eliminates fluctuations in the collection efficiency of C_4+. The use of SiC resulted in 22% deoxygenation while preserving 88% of the energy of condensable products. For all catalysts, at 500 °C the energy recovery of condensable vapors decreased with increasing deoxygenation severity. At 500 °C, the desilicated HZSM-5/Al_2O_3 extrudate achieved ~5-10% deeper deoxygenation of condensable vapors compared to the other catalysts. The carbon recovery in the oil phase was 24.2 %at B:C = 6.3, while removing 45% of the oxygen functionalities relative to the SiC oil.

When using ZSM-5 based catalysts (alone or as extrudates with Al_2O_3) it does not appear attractive to aim for deep deoxygenation and high aromatics yield since the overall drop in oil yield is high considering the low product yields of BTX. Instead, production of fuel grade chemicals appears more favorable and one should aim for sufficient deoxygenation to get a stable oil with reduced acidity. The acidity of the oils is clearly correlated with the oxygen content (see Fig. S15), and thus also the carbon recovery of the oil (see **Figure 8**). As such, the TAN should only be reduced to an extent that allows further (co-) processing in FCC or hydrotreating processes. Mante et al.[53] demonstrated that bio-oil with 19.5 wt-% O produced by upgrading of pine pyrolysis vapors with a nonzeolite, alumina-based catalyst at ~520 °C could be successfully upgraded into hydrocarbon liquid fuels in a single-stage hydrotreating. Utilizing Al_2O_3 at 450-500 °C therefore appears to be an economically attractive alternative compared to using HZSM-5 based catalysts.

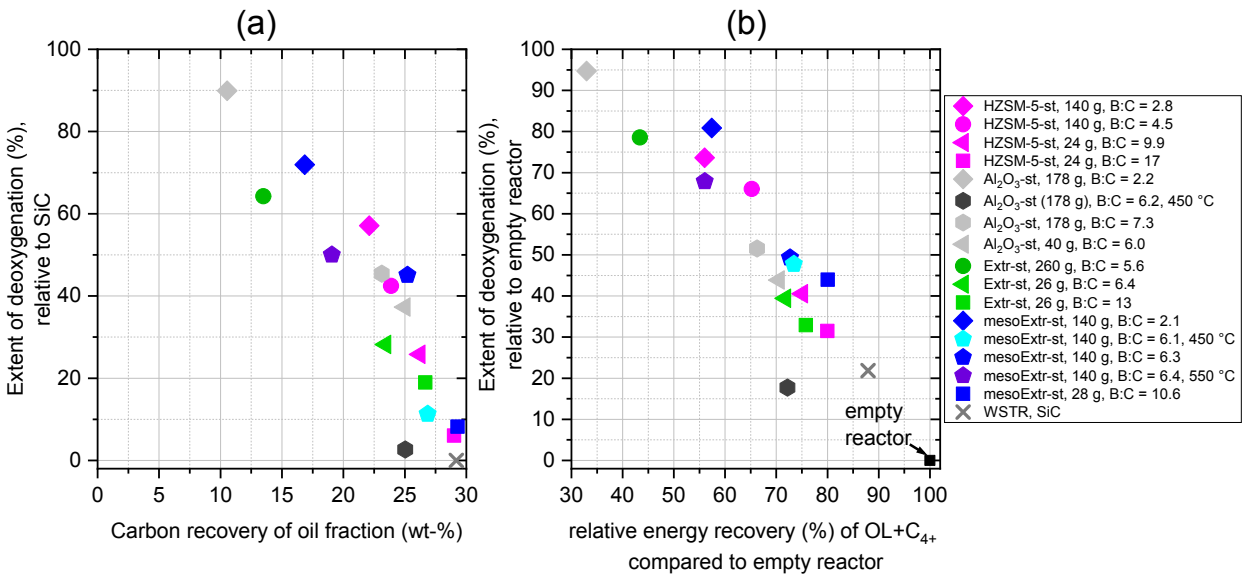

Figure 8. (a) Shows the carbon recovery in the phase separated oil fraction and the extent of deoxygenation relative to SiC oil with 21.5 wt-% O (d.b.). (b) Shows the deoxygenation and energy recovery of the condensable vapors, that is organic liquid (OF + WF) and C_4+ gas compounds, relative to results obtained with an empty reactor. Catalyst temperature was 500 °C unless noted otherwise in the figure legend (applies for both graphs). For interpretation of the references to color in this figure legend, the reader is referred to the web version of this article.

Conclusion

We demonstrated what yields of deoxygenated pyrolysis oil can be obtained from ex-situ catalytic straw fast pyrolysis using steam treated HZSM-5, alumina binder, HZSM-5/Al_2O_3 extrudates, and mesoporous HZSM-5/ Al_2O_3 extrudates obtained by desilication of the original extrudates. At 500 °C, all catalysts reduced the oil yield but improved the oil quality in terms of reduced moisture and oxygen content, TAN, improved evaporation characteristics and lower molecular weight. A reduction in the catalyst temperature from 500 to 450 °C clearly reduced the deoxygenation activity, especially for alumina. While alumina showed the highest coking propensity, its

deoxygenation performance at 500 °C was comparable to the HZSM-5 based catalysts, which makes it economically attractive.

Desilication allowed introducing mesopores to the zeolitic phase of HZSM-5/Al_2O_3 extrudates without disintegration of the extrudates. Despite achieving ~8% higher deoxygenation compared to conventional HZSM-5 or alumina at a carbon recovery of ~25% of the oil phase, the benefit of the added mesoporosity will have to justify the costs associated with the additional treatment. Overall, the approach of mild rather than deep deoxygenation appears more viable for treating the pyrolysis vapors before co-processing the condensed bio-oil with fossil oil in refineries.

ASSOCIATED CONTENT

Supporting Information: NH_3-TPD profiles; XRF elemental analysis; CO/CO_2 ratio during reaction; TGA simulated distillation curves; correlation of charring tendency with oxygen content of oils; elemental analysis of liquids; molar H/C ratio and O/C ratio of oils obtained with Al_2O_3 and mesoporous HZSM-5 extrudates at different temperatures; monoaromatics selectivity; ^1H NMR spectra; ^{13}C NMR; build-up of coke on steamed HZSM-5/Al_2O_3 and steamed mesoporous HZSM-5/Al_2O_3; carbon product distribution

AUTHOR INFORMATION

Corresponding Author

* aj@kt.dtu.dk

Funding Sources

Partial funding by the Energy Technology Development and Demonstration Program (EUDP project number 12454) of the Ph.D. project conducted at the CHEC Research Center, DTU Chemical Engineering, is acknowledged.

ACKNOWLEDGMENT

Lotte Nielsen is acknowledged for conducting the SEC analysis at the DTU Department of Micro- and Nanotechnology. Peter Wiwel (Haldor Topsøe) is acknowledged for conducting the total sulfur determination of bio-oil samples.

ABBREVIATIONS

CFP, catalytic fast pyrolysis; daf, dry ash-free basis; d.b., dry basis, DRI, differential refractive index; ESI, electronic supporting information; ESP, electrostatic precipitator; FID, flame ionization detection; FP, fast pyrolysis; GC, gas chromatography; HHV, higher heating value; HSQC, heteronuclear single-quantum correlation; ID, inner diameter; MS, mass spectrometry; n.d., not determined; NMR; nuclear magnetic resonance; SEC, size exclusion chromatography; TAN, total acid number; TEM, transmission electron microscopy; TGA, thermogravimetric analysis; TPD, temperature-programmed desorption; OF, oil fraction obtained by spontaneous phase separation; OL, organic liquid; WF, water fraction obtained by spontaneous phase separation; XRF, X-ray fluorescence;

REFERENCES

(1) Huber, G. W.; Corma, A. Synergies between Bio- and Oil Refineries for the Production of Fuels from Biomass. *Angew. Chemie - Int. Ed.* **2007**, *46* (38), 7184–7201. https://doi.org/10.1002/anie.200604504.

(2) Case, P. A.; Wheeler, M. C.; DeSisto, W. J. Effect of Residence Time and Hot Gas Filtration on the Physical and Chemical Properties of Pyrolysis Oil. *Energy and Fuels* **2014**, *28* (6),

3964–3969. https://doi.org/10.1021/ef500850y.

(3) Krutof, A.; Hawboldt, K. A. Upgrading of Biomass Sourced Pyrolysis Oil Review: Focus on Co-Pyrolysis and Vapour Upgrading during Pyrolysis. *Biomass Convers. Biorefinery* **2018**, *8* (3), 775–787. https://doi.org/10.1007/s13399-018-0326-6.

(4) Bridgwater, A. V.; Peacocke, G. V. C. Fast Pyrolysis Processes for Biomass. *Renew. Sustain. Energy Rev.* **2000**, *4* (1), 1–73. https://doi.org/10.1016/S1364-0321(99)00007-6.

(5) French, R.; Czernik, S. Catalytic Pyrolysis of Biomass for Biofuels Production. *Fuel Process. Technol.* **2010**, *91* (1), 25–32. https://doi.org/10.1016/j.fuproc.2009.08.011.

(6) Jae, J.; Tompsett, G. A.; Foster, A. J.; Hammond, K. D.; Auerbach, S. M.; Lobo, R. F.; Huber, G. W. Investigation into the Shape Selectivity of Zeolite Catalysts for Biomass Conversion. *J. Catal.* **2011**, *279* (2), 257–268. https://doi.org/10.1016/j.jcat.2011.01.019.

(7) Carlson, T. R.; Tompsett, G. A.; Conner, W. C.; Huber, G. W. Aromatic Production from Catalytic Fast Pyrolysis of Biomass-Derived Feedstocks. *Top. Catal.* **2009**, *52* (3), 241–252. https://doi.org/10.1007/s11244-008-9160-6.

(8) Choudhary, V. R.; Devadas, P.; Kinage, a. K.; Guisnet, M.; Sciences, U. D. P. Influence of Binder on the Acidity and Performance of H-Gallosilicate (MFI) Zeolite in Propane Aromatization. *Appl. Catal. A Gen.* **1997**, *162* (1–2), 223–233. https://doi.org/10.1016/S0926-860X(97)00100-2.

(9) Michels, N.-L.; Mitchell, S.; Pérez-Ramírez, J. Effects of Binders on the Performance of Shaped Hierarchical MFI Zeolites in Methanol-to-Hydrocarbons. *ACS Catal.* **2014**, *4* (8), 2409–2417. https://doi.org/10.1021/cs500353b.

(10) Gueudré, L.; Milina, M.; Mitchell, S.; Pérez-Ramírez, J. Superior Mass Transfer Properties of Technical Zeolite Bodies with Hierarchical Porosity. *Adv. Funct. Mater.* **2014**, *24* (2),

209–219. https://doi.org/10.1002/adfm.201203557.

(11) Michels, N.-L.; Mitchell, S.; Milina, M.; Kunze, K.; Krumeich, F.; Marone, F.; Erdmann, M.; Marti, N.; Pérez-Ramírez, J. Hierarchically Structured Zeolite Bodies: Assembling Micro-, Meso-, and Macroporosity Levels in Complex Materials with Enhanced Properties. *Adv. Funct. Mater.* **2012**, *22* (12), 2509–2518. https://doi.org/10.1002/adfm.201103120.

(12) Iisa, K.; French, R.; Orton, K. A.; Budhi, S.; Mukarakate, C.; Stanton, A. R.; Yung, M. M.; Nimlos, M. R. Catalytic Pyrolysis of Pine over HZSM-5 with Different Binders. *Top. Catal.* **2016**, *59* (1), 94–108. https://doi.org/10.1007/s11244-015-0509-3.

(13) Du, S.; Gamliel, D. P.; Valla, J. A.; Bollas, G. M. The Effect of ZSM-5 Catalyst Support in Catalytic Pyrolysis of Biomass and Compounds Abundant in Pyrolysis Bio-Oils. *J. Anal. Appl. Pyrolysis* **2016**, *122*, 7–12. https://doi.org/10.1016/j.jaap.2016.11.002.

(14) Murillo, B. L.; Pala, M.; Prins, W.; Ronsse, F.; Bruijnincx, P. C. A.; Weckhuysen, B. M. Advanced Characterization of HZSM-5/Al2O3 Extrudates after Catalytic Fast Pyrolysis of Biomass. In *Symposium on Thermal and Catalytic Sciences for Biofuels and Biobased Products*; 2018.

(15) Stefanidis, S. D.; Kalogiannis, K. G.; Iliopoulou, E. F.; Lappas, A. A.; Pilavachi, P. A. In-Situ Upgrading of Biomass Pyrolysis Vapors: Catalyst Screening on a Fixed Bed Reactor. *Bioresour. Technol.* **2011**, *102* (17), 8261–8267. https://doi.org/10.1016/j.biortech.2011.06.032.

(16) Yorgun, S.; Şimşek, Y. E. Catalytic Pyrolysis of Miscanthus × Giganteus over Activated Alumina. *Bioresour. Technol.* **2008**, *99* (17), 8095–8100. https://doi.org/10.1016/j.biortech.2008.03.036.

(17) Ateş, F.; Işikdağ, M. A. Influence of Temperature and Alumina Catalyst on Pyrolysis of

889 Corncob. *Fuel* **2009**, *88* (10), 1991–1997. https://doi.org/10.1016/j.fuel.2009.03.008.

890 (18) Demiral, I.; Şensöz, S. The Effects of Different Catalysts on the Pyrolysis of Industrial
891 Wastes (Olive and Hazelnut Bagasse). *Bioresour. Technol.* **2008**, *99* (17), 8002–8007.
892 https://doi.org/10.1016/j.biortech.2008.03.053.

893 (19) Samolada, M. C.; Papafotica, A.; Vasalos, I. A. Catalyst Evaluation for Catalytic Biomass
894 Pyrolysis. *Energy & Fuels* **2000**, *14* (6), 1161–1167. https://doi.org/10.1021/ef000026b.

895 (20) Zhang, H.; Xiao, R.; Jin, B.; Xiao, G.; Chen, R. Biomass Catalytic Pyrolysis to Produce
896 Olefins and Aromatics with a Physically Mixed Catalyst. *Bioresour. Technol.* **2013**, *140*,
897 256–262. https://doi.org/10.1016/j.biortech.2013.04.094.

898 (21) Wang, K.; Mante, O.; Peters, J. E.; Dayton, D. C. Influence of the Feedstock on Catalytic
899 Fast Pyrolysis with a Solid Acid Catalyst. *Energy Technol.* **2017**, *5* (1), 183–188.
900 https://doi.org/10.1002/ente.201600254.

901 (22) Mante, O.; Dayton, D. C.; Carpenter, J. R.; Wang, K.; Peters, J. E. Pilot-Scale Catalytic Fast
902 Pyrolysis of Loblolly Pine over y-Al2O3 Catalyst. *Fuel* **2018**, *214* (September 2017), 569–
903 579. https://doi.org/10.1016/j.fuel.2017.11.073.

904 (23) Ik, H.; Ju, H.; Park, Y. K.; Young, J.; Jeon, J.; Man, J. Synthesis of Highly Stable
905 Mesoporous Aluminosilicates from Commercially Available Zeolites and Their Application
906 to the Pyrolysis of Woody Biomass. *Catal. Today* **2008**, *132*, 68–74.
907 https://doi.org/10.1016/j.cattod.2007.12.029.

908 (24) Park, H. J.; Heo, H. S.; Jeon, J. K.; Kim, J.; Ryoo, R.; Jeong, K. E.; Park, Y.-K. K.; Ju, H.;
909 Su, H. Highly Valuable Chemicals Production from Catalytic Upgrading of Radiata Pine
910 Sawdust-Derived Pyrolytic Vapors over Mesoporous MFI Zeolites. *Appl. Catal. B Environ.*
911 **2010**, *95* (3–4), 365–373. https://doi.org/10.1016/j.apcatb.2010.01.015.

(25) Jia, L. Y.; Raad, M.; Hamieh, S.; Toufaily, J.; Hamieh, T.; Bettahar, M. M.; Mauviel, G.; Tarrighi, M.; Pinard, L.; Dufour, A. Catalytic Fast Pyrolysis of Biomass: Superior Selectivity of Hierarchical Zeolites to Aromatics. *Green Chem.* **2017**, *19* (22), 5442–5459. https://doi.org/10.1039/c7gc02309j.

(26) Puértolas, B.; Veses, A.; Callén, M. S.; Mitchell, S.; García, T.; Pérez-Ramírez, J. Porosity-Acidity Interplay in Hierarchical ZSM-5 Zeolites for Pyrolysis Oil Valorization to Aromatics. *ChemSusChem* **2015**, *8* (19), 3283–3293. https://doi.org/10.1002/cssc.201500685.

(27) Michels, N.-L. From Powder to Technical Body : Structured Zeolite Catalysts with Enhanced Functionality, ETH Zurich, 2014.

(28) Groen, J. C.; Moulijn, J. A.; Pérez-Ramírez, J. Alkaline Posttreatment of MFI Zeolites. From Accelerated Screening to Scale-Up. *Ind. Eng. Chem. Res.* **2007**, *46* (12), 4193–4201. https://doi.org/10.1021/ie061146v.

(29) Eschenbacher, A.; Jensen, P. A.; Henriksen, U. B.; Ahrenfeldt, J.; Li, C.; Duus, J. Ø.; Mentzel, U. V.; Jensen, A. D. Impact of ZSM-5 Deactivation on Bio-Oil Quality during Upgrading of Straw Derived Pyrolysis Vapors. *Energy & Fuels* **2019**, *33* (1), 397–412. https://doi.org/10.1021/acs.energyfuels.8b03691.

(30) Lignin, C.; Pyrolysis, S. F.; Trinh, T. N.; Jensen, P. A.; Dam-johansen, K.; Knudsen, N. O.; Sørensen, H. R.; Hvilsted, S. Comparison of Lignin, Macroalgae, Wood, and Straw Fast Pyrolysis. **2013**.

(31) Groen, J. C.; Peffer, L. A. A.; Moulijn, J. A.; Pérez-Ramírez, J. Mesoporosity Development in ZSM-5 Zeolite upon Optimized Desilication Conditions in Alkaline Medium. *Colloids Surfaces A Physicochem. Eng. Asp.* **2004**, *241* (1–3), 53–58.

https://doi.org/10.1016/j.colsurfa.2004.04.012.

(32) Groen, J. C.; Moulijn, J. a.; Peréz-Ramírez, J. Desilication: On the Controlled Generation of Mesoporosity in MFI Zeolites. *J. Mater. Chem.* **2006**, *16* (22), 2121. https://doi.org/10.1039/b517510k.

(33) Bates, S. A.; Delgass, W. N.; Ribeiro, F. H.; Miller, J. T.; Gounder, R. Methods for NH3titration of Brønsted Acid Sites in Cu-Zeolites That Catalyze the Selective Catalytic Reduction of NOxwith NH3. *J. Catal.* **2014**, *312*, 26–36. https://doi.org/10.1016/j.jcat.2013.12.020.

(34) Abdelrahman, O. A.; Vinter, K. P.; Ren, L.; Xu, D.; Gorte, R. J.; Tsapatsis, M.; Dauenhauer, P. J. Simple Quantification of Zeolite Acid Site Density by Reactive Gas Chromatography. *Catal. Sci. Technol.* **2017**, *7* (17), 3831–3841. https://doi.org/10.1039/c7cy01068k.

(35) Kresnawahjuesa, O.; Gorte, R. J.; De Oliveira, D.; Lau, L. Y. A Simple, Inexpensive, and Reliable Method for Measuring Brønsted-Acid Site Densities in Solid Acids. *Catal. Letters* **2002**, *82* (3–4), 155–160. https://doi.org/10.1023/A:1020514911456.

(36) Thommes, M.; Guillet-Nicolas, R.; Cychosz, K. A. Physical Adsorption Characterization of Mesoporous Zeolites. *Mesoporous Zeolites Prep. Charact. Appl.* **2015**, 349–384. https://doi.org/10.1002/9783527673957.ch11.

(37) Mohammed, I. Y.; Abakr, Y. A.; Yusup, S.; Alaba, P. A.; Morris, K. I.; Sani, Y. M.; Kazi, F. K. Upgrading of Napier Grass Pyrolytic Oil Using Microporous and Hierarchical Mesoporous Zeolites: Products Distribution, Composition and Reaction Pathways. *J. Clean. Prod.* **2017**, *162*, 817–829. https://doi.org/10.1016/j.jclepro.2017.06.105.

(38) Malysheva, L. V.; Paukshtis, E. A.; Kotsarenko, N. S. Mechanism of Deamination of Butylamines on Protonic Centers of HNaY Zeolite. *J. Catal.* **1987**, *104* (1), 31–36.

https://doi.org/10.1016/0021-9517(87)90333-2.

(39) Mohammed, I. Y.; Kazi, F. K.; Yusup, S.; Alaba, P. A.; Sani, Y. M.; Abakr, Y. A. Catalytic Intermediate Pyrolysis of Napier Grass in a Fixed Bed Reactor with ZSM-5, HZSM-5 and Zinc-Exchanged Zeolite-a as the Catalyst. *Energies* **2016**, *9* (4). https://doi.org/10.3390/en9040246.

(40) Leflaive, P.; Lemberton, J. L.; Pérot, G.; Mirgain, C.; Carriat, J. Y.; Colin, J. M. On the Origin of Sulfur Impurities in Fluid Catalytic Cracking Gasoline - Reactivity of Thiophene Derivatives and of Their Possible Precursors under FCC Conditions. *Appl. Catal. A Gen.* **2002**, *227* (1–2), 201–215. https://doi.org/10.1016/S0926-860X(01)00936-X.

(41) Zhang, H.; Xiao, R.; Jin, B.; Shen, D.; Chen, R.; Xiao, G. Catalytic Fast Pyrolysis of Straw Biomass in an Internally Interconnected Fluidized Bed to Produce Aromatics and Olefins: Effect of Different Catalysts. *Bioresour. Technol.* **2013**, *137*, 82–87. https://doi.org/10.1016/j.biortech.2013.03.031.

(42) Iliopoulou, E. F.; Stefanidis, S. D.; Kalogiannis, K. G.; Delimitis, A.; Lappas, A. A.; Triantafyllidis, K. S. Catalytic Upgrading of Biomass Pyrolysis Vapors Using Transition Metal-Modified ZSM-5 Zeolite. *Appl. Catal. B Environ.* **2012**, *127*, 281–290. https://doi.org/10.1016/j.apcatb.2012.08.030.

(43) Balasundram, V.; Ibrahim, N.; Kasmani, R. M.; Isha, R.; Hamid, M. K. A.; Hasbullah, H.; Ali, R. R. Catalytic Upgrading of Sugarcane Bagasse Pyrolysis Vapours over Rare Earth Metal (Ce) Loaded HZSM-5: Effect of Catalyst to Biomass Ratio on the Organic Compounds in Pyrolysis Oil. *Appl. Energy* **2018**, *220* (December 2017), 787–799. https://doi.org/10.1016/j.apenergy.2018.03.141.

(44) Zhang, M.; Resende, F. L. P.; Moutsoglou, A. Catalytic Fast Pyrolysis of Aspen Lignin via

Py-GC/MS. *Fuel* **2014**, *116*, 358–369. https://doi.org/10.1016/j.fuel.2013.07.128.

(45) Stanton, A. R.; Iisa, K.; Mukarakate, C.; Nimlos, M. R. Role of Biopolymers in the Deactivation of ZSM-5 during Catalytic Fast Pyrolysis of Biomass. *ACS Sustain. Chem. Eng.* **2018**, *6* (8), 10030–10038. https://doi.org/10.1021/acssuschemeng.8b01333.

(46) Mante, O.; Agblevor, F. A.; Oyama, S. T.; McClung, R. The Effect of Hydrothermal Treatment of FCC Catalysts and ZSM-5 Additives in Catalytic Conversion of Biomass. *Appl. Catal. A Gen.* **2012**, *445–446*, 312–320. https://doi.org/10.1016/j.apcata.2012.08.039.

(47) Joseph, J.; Baker, C.; Mukkamala, S.; Beis, S. H.; Wheeler, M. C.; DeSisto, W. J.; Jensen, B. L.; Frederick, B. G. Chemical Shifts and Lifetimes for Nuclear Magnetic Resonance (NMR) Analysis of Biofuels. *Energy & Fuels* **2010**, *24* (9), 5153–5162. https://doi.org/10.1021/ef100504d.

(48) Ong, L. H.; Dömök, M. M.; Olindo, R.; Veen, A. C. Van; Lercher, J. A.; van Veen, A. C.; Lercher, J. A. Dealumination of HZSM-5 via Steam-Treatment. *Microporous Mesoporous Mater.* **2012**, *164*, 9–20. https://doi.org/10.1016/j.micromeso.2012.07.033.

(49) Du, S.; Sun, Y.; Gamliel, D. P.; Valla, J. A.; Bollas, G. M. Catalytic Pyrolysis of Miscanthus×giganteus in a Spouted Bed Reactor. *Bioresour. Technol.* **2014**, *169*, 188–197. https://doi.org/10.1016/j.biortech.2014.06.104.

(50) Channiwala, S. A.; Parikh, P. P. A Unified Correlation for Estimating HHV of Solid, Liquid and Gaseous Fuels. *Fuel* **2002**, *81* (8), 1051–1063. https://doi.org/10.1016/S0016-2361(01)00131-4.

(51) Tröger, N.; Richter, D.; Stahl, R. Effect of Feedstock Composition on Product Yields and Energy Recovery Rates of Fast Pyrolysis Products from Different Straw Types. *J. Anal. Appl. Pyrolysis* **2013**, *100*, 158–165. https://doi.org/10.1016/j.jaap.2012.12.012.

(52) Puørtolas, B.; Veses, A.; Calløn, S.; Mitchell, S.; García, T.; Pørez-ramírez, J. Porosity – Acidity Interplay in Hierarchical ZSM-5 Zeolites for Pyrolysis Oil Valorization to Aromatics. **2015**, 3283–3293. https://doi.org/10.1002/cssc.201500685.

(53) Mante, O. D.; Dayton, D. C.; Gabrielsen, J.; Ammitzboll, N. L.; Barbee, D.; Verdier, S.; Wang, K. Integration of Catalytic Fast Pyrolysis and Hydroprocessing: A Pathway to Refinery Intermediates and "Drop-in" Fuels from Biomass. *Green Chem.* **2016**, *18* (22), 6123–6135. https://doi.org/10.1039/c6gc01938b.